

# UC Irvine

## UC Irvine Previously Published Works

### Title

EIF1AX and RAS mutations cooperate to drive thyroid tumorigenesis through ATF4 and c-MYC

### Permalink

<https://escholarship.org/uc/item/03c5s4cv>

### Journal

Cancer Discovery, 9(2)

### ISSN

2159-8274

### Authors

Krishnamoorthy, Gnana P  
Davidson, Natalie R  
Leach, Steven D  
[et al.](#)

### Publication Date

2019-02-01

### DOI

10.1158/2159-8290.cd-18-0606

Peer reviewed



Published in final edited form as:

*Cancer Discov.* 2019 February ; 9(2): 264–281. doi:10.1158/2159-8290.CD-18-0606.

## ***EIF1AX* and *RAS* mutations cooperate to drive thyroid tumorigenesis through ATF4 and c-MYC**

Gnana P. Krishnamoorthy<sup>1</sup>, Natalie R. Davidson<sup>2</sup>, Steven D. Leach<sup>1</sup>, Zhen Zhao<sup>3</sup>, Scott W. Lowe<sup>3</sup>, Gina Lee<sup>6</sup>, Iigo Landa<sup>1</sup>, James Nagarajah<sup>1</sup>, Mahesh Saqcena<sup>1</sup>, Kamini Singh<sup>3</sup>, Hans-Guido Wendel<sup>3</sup>, Snjezana Dogan<sup>5</sup>, Prasanna P. Tamarapu<sup>1</sup>, John Blenis<sup>6</sup>, Ronald A. Ghossein<sup>5</sup>, Jeffrey A. Knauf<sup>1,4</sup>, Gunnar Rättsch<sup>2</sup>, and James A. Fagin<sup>1,4</sup>

<sup>1</sup>Human Oncology and Pathogenesis Program, Memorial Sloan Kettering Cancer Center, New York, NY, U.S.A.

<sup>2</sup>Computational Biology Program, Memorial Sloan Kettering Cancer Center, New York, NY, U.S.A.

<sup>3</sup>Cancer Biology and Genetics Program, Memorial Sloan Kettering Cancer Center, New York, NY, U.S.A.

<sup>4</sup>Department of Medicine, Memorial Sloan Kettering Cancer Center, New York, NY, U.S.A.

<sup>5</sup>Department of Pathology, Memorial Sloan Kettering Cancer Center, New York, NY, U.S.A.

<sup>6</sup>Department of Pharmacology, Meyer Cancer Center, Weill Cornell Medicine, New York, NY, U.S.A.

### **Abstract**

Translation initiation is orchestrated by the cap binding and 43S pre-initiation complexes (PIC). Eukaryotic initiation factor 1A (EIF1A) is essential for recruitment of the ternary complex and for assembling the 43S PIC. Recurrent *EIF1AX* mutations in papillary thyroid cancers are mutually exclusive with other drivers, including *RAS*. *EIF1AX* is enriched in advanced thyroid cancers, where it displays a striking co-occurrence with *RAS*, which cooperates to induce tumorigenesis in mice and isogenic cell lines. The C-terminal *EIF1AX-A113splice* mutation is the most prevalent in advanced thyroid cancer. *EIF1AX-A113spl* variants stabilize the PIC and induce ATF4, a sensor of cellular stress, which is co-opted to suppress EIF2 $\alpha$  phosphorylation, enabling a general increase in protein synthesis. *RAS* stabilizes c-MYC, an effect augmented by *EIF1AX-A113spl*. ATF4 and c-MYC induce expression of aminoacid transporters and enhance sensitivity of mTOR to aminoacid supply. These mutually reinforcing events generate therapeutic vulnerabilities to MEK, BRD4 and mTOR kinase inhibitors.

---

**Correspondence:** James A. Fagin, MD, Department of Medicine and Human Oncology and Pathogenesis Program,, Memorial Sloan-Kettering Cancer Center, 1275 York Avenue, New York, NY 10065, U.S.A., faginj@mskcc.org.

“The authors declare no potential conflicts of interest.”

Data availability.

Ribosome profiling and RNA sequencing data from this study have been submitted to the NCBI Gene Expression Omnibus under accession number GSE113695.

## Introduction

Papillary carcinomas (PTC) are the most common type of thyroid cancer. They are usually indolent tumors that harbor mutually exclusive mutations in *BRAF*, *RAS* or fusions of *RET*, *NTRK* or *BRAF* (1–3). The TCGA study of PTC identified additional driver alterations present at lower frequency, including *EIF1AX*, *PPM1D* and *CHEK2* (4). Poorly differentiated (PDTC) and anaplastic thyroid cancers (ATC) are the most aggressive forms of the disease and are characterized by distinct genomic profiles. Although *BRAF* and *RAS* mutations are also the main drivers, as compared to PTC they are more frequently associated with mutations of the *TERT* promoter, *TP53*, genes encoding PI3K/AKT/mTOR pathway effectors or chromatin modifiers (5–7). They are also markedly enriched for *EIF1AX* mutations.

Translation initiation in higher eukaryotes is orchestrated by the tight regulation of the cap binding and the 43S pre-initiation complexes (PIC). Formation of the PIC involves recruitment of the ternary complex (EIF2-GTP-tRNA<sup>i</sup>(Met)) onto the 40S ribosomal subunit. The PIC component EIF1A, which is encoded on human chromosomes X and Y by *EIF1AX* and *EIF1AY*, respectively. Their protein products are highly conserved, and expression of EIF1A is biallelic irrespective of gender (8,9). EIF1A is required for recruitment of the ternary complex and for assembling the 43S PIC (10), which after recruitment onto capped mRNAs scans their 5'UTR and localizes the AUG to initiate translation (11,12). Deregulation of translation initiation is common in tumorigenesis. Increased expression of components of the EIF4F cap binding complex (*EIF4E*, *EIF4A*, *EIF4G*) is seen in many cancers. The expression of these genes is under transcriptional control by c-MYC (13,14). EIF4E is limiting for translating the mammalian genome, and is frequently found in excess in cancer cells, where it may help drive a translational output supporting tumorigenesis (15).

To our knowledge *EIF1AX* is the only example of a PIC subunit recurrently mutated in cancer. Mutations of *EIF1AX* were first reported in uveal melanomas (8). Comprehensive genomic profiling of these tumors revealed that *EIF1AX*-mutant tumors mark a comparatively low risk form of the disease. *EIF1AX* and *GNA11/GNAQ* mutations frequently co-occurred and were mutually exclusive with c-MYC amplification (16). *EIF1AX* mutations have been reported in benign thyroid adenomas (17), follicular carcinomas (18) as well as in ~1% of PTC in a mutually exclusive manner with other drivers (4). By contrast, they are present in 11% of PDTC and ATC, and are almost invariably associated with oncogenic *RAS* (5,7). The striking co-evolution of *EIF1AX* and *RAS* mutations in advanced disease suggests that they may cooperate to drive tumor progression.

The core RNA binding domain of *EIF1A* is universally conserved from archaea to eukaryotes, whereas eukaryotes differ from bacteria by the addition of the unstructured amino-terminal (NTT) and carboxy-terminal tails (CTT) (19,20). *EIF1AX* mutations identified in several cancers encode somatic substitutions in the first 2–15 amino acids of the NTT (8,21,22), whereas thyroid cancers harbour an additional hotspot splice site mutation (*EIF1AX-A113splice*) in the CTT that is private to this disease (4,5,7). *EIF1AX* mutations are always heterozygous, suggesting that full occupancy of PICs by mutant EIF1AX would

be detrimental to viability. Structure-function studies in yeast revealed that mutating any of the NTT residues between 7 and 16 amino acid were lethal and resulted in leaky scanning of the initiation AUG codon (23,24), and discriminated against AUGs with poor context (25). By contrast, CTT mutants enhanced non-canonical AUG initiations. Of note, the experimental CTT substitutions tested in yeast did not appropriately model the structural defects of the *EIF1AX* splice site mutation (*A113splice*).

Here we describe the identification of the key signaling drivers of transformation by *EIF1AX* mutants, particularly *EIF1AX-A113splice*, alone and in the context of RAS, and the therapeutic dependencies they confer.

## Results

### ***EIF1AX* mutation is a strong co-operating event with RAS in advanced thyroid cancer; the hotspot A113splice mutation induces aberrant splice variants.**

Analysis of our institutional clinical genomics database of 148 advanced thyroid cancers coupled to data from two previously published studies (5,7) showed that 26/246 (11%) tumors harbored *EIF1AX* mutations, 25 of which were associated with mutant *RAS* (25/26;  $p=3.15 \times 10E^{-13}$ ) (Fig. 1A). The *EIF1AX* mutations clustered within the first 15 amino acids of the N-terminal tail (NTT), as reported in uveal melanomas (8), or more frequently at a hotspot splice acceptor site upstream of exon 6 (*A113splice*) in the C-terminal tail (CTT) (17/26) (Fig. 1A). The *A113splice* mutation, not seen so far in any other cancer type, abolished the acceptor site of exon 6, resulting in two alternatively spliced transcripts (Fig. 1B): i) c'splice, through usage of a cryptic site within exon 6, yielding a 132AA protein through an in-frame exclusion of 12 AA. ii) t'splice, which retains intron 5, resulting in a 115AA truncated protein. We confirmed the presence of these alternatively spliced mRNA's in the RNAseq data of *A113splice*-mutant PTCs from the TCGA study (4) (Supplementary Fig. S1A). Western blotting of HTH83 and C643 thyroid cancer cell lines harboring the *A113splice* mutation showed *EIF1AX* protein products corresponding to c'spl and t'spl mRNAs, with c'spl as the predominantly expressed isoform (Fig. 1C). Their predicted AA sequences are shown in Supplementary Fig. S1B.

### **Aberrant splice variants of *EIF1AX-A113splice* mutation induce transformation *in vitro*.**

To explore the biological consequences of the *EIF1AX-A113splice* mutation, either alone or in the context of mutant *RAS*, we generated isogenic thyroid cancer cell lines by CRISPR-Cas9 knock-in of heterozygous mutations of *A113splice* into *KRAS*<sup>G12R</sup>-mutant CAL62 or *RAS*-wild type TTA1 cells, and by reversing the endogenous *A113splice* mutation in *HRAS*<sup>G13R</sup> and *EIF1AX*<sup>A113spl</sup>-mutant C643 cells (Fig. 2A, Supplementary Fig. S2A and S2B). Introduction of *A113splice* into CAL62 or TTA1 cells markedly increased their colony formation in soft agar, whereas transformation efficiency was decreased by editing out *A113splice* in C643 cells (Fig. 2A). We then tested the effects of the two *EIF1AX-A113splice* products, c'spl and t'spl, independently and in combination on transformation of Nthy-Ori 3-1 cells, an SV40 large-T-antigen immortalized human thyroid cell line. The c'spl product markedly increased colony formation, whereas the t'spl did not, and dampened

the effects of c'spl when both were co-expressed through a bicistronic vector, consistent with EIF1AX-c'spl being the functionally active variant (Supplementary Fig. S2C).

### **EIF1AX-c-splice cooperates with oncogenic Ras to induce disease progression in genetically engineered mice.**

We next investigated the interaction of oncogenic Hras and EIF1AX-c'spl *in vivo*. For this we generated mice with thyroid-specific, doxycycline (dox)-inducible expression of EIF1AX-c'spl by targeting a *TRE-EIF1AX-c'spl* construct into the mouse *Col1A1* locus and crossing the resulting animals with *Tg-rtTA* mice (Fig. 2B). Dox-fed *Tg-rtTA/TRE-EIF1AX-c'spl* mice expressed the c'spl protein in thyroid tissue (Fig. 2C), which developed thyrocyte hyperplasia with atypical features (18/19), with one animal developing a low-grade classical PTC (Fig. 2D and 2E). These findings closely phenocopy the human thyroid histologies associated with an isolated *EIF1AX* mutation (4,17). *TPO-Cre/FR-Hras<sup>G12V</sup>* mice express Hras<sup>G12V</sup> upon Cre-induced recombination in the thyroid (Fig. 2B), which is insufficient to drive tumorigenesis (26). By contrast, the quadri-transgenics (*TPO-Cre/FR-Hras<sup>G12V</sup>/Tg-rtTA/TRE-EIF1AX-c'spl*) displayed neoplasms along the spectrum of disease progression with a penetrance of 30%, including Hurthle cell adenoma, PTC and PDTC (Fig. 2D and 2E, Supplementary Fig. S2D), consistent with the histological characteristics of human thyroid tumors harboring the combined genetic lesions (17).

### **EIF1AX mutants have higher affinity to components of the translation PIC and increase protein synthesis.**

EIF1AX is an essential subunit of the translation PIC (10,12). We performed co-immunoprecipitation experiments to probe for possible aberrant interactions of EIF1AX mutants with components of the ternary complex (TC) and the PIC. IP of HEK293T cells expressing HA-tagged wild-type (WT) EIF1AX, NTT mutants (G8R, G9R, G15V) or EIF1AX-c'spl with an antibody to HA showed pulldown of the TC component eukaryotic initiation factor 2 $\alpha$  (EIF2 $\alpha$ ) by all EIF1AX proteins, with EIF1AX-c'spl showing greater affinity (Fig. 3A). IP of the HEK293T lysates with EIF5, a component of the PIC, did not detect EIF1AX-WT in the immunoprecipitate, likely because of the known labile interactions between these PIC subunits (10). By contrast, EIF1AX mutants, particularly G8R, G9R and c'spl, exhibited increased affinity for EIF5 (Fig. 3B), consistent with stabilization of the PIC. This was confirmed in the isogenic EIF1AX-splice cell lines (Fig. 3C), and in thyroid cancer cells with endogenous *EIF1AX* mutations (Supplementary Fig. S3A). These data suggest that EIF1AX mutants result in a more stable 43S ribosomal complex. As translation initiation is a rate limiting process, we next tested whether the EIF1AX mutants altered nascent protein synthesis in the isogenic lines. L-azidohomoalanine (AHA)-labeled proteins were markedly increased by knock-in of the *A113splice* mutation into *RAS* wild type (TTA1) or mutant cells (CAL62), whereas reversion of the mutation in C643-spl-rev cells had the opposite effect (Fig. 3D and 3E). NthyOri cells stably expressing EIF1AX-G8R, G9R or EIF1AX-c'spl also showed an increase in nascent protein synthesis compared to WT, with c'spl having the greatest effect (Fig. 3D and 3E). The increased protein synthesis by c'spl is comparable to that induced by EIF4E overexpression (Supplementary Fig. S3B) and is blocked by mTOR kinase inhibition (Supplementary Fig. S3C).

### Increased global protein synthesis by EIF1AX-splice is mediated by ATF4-induced EIF2 $\alpha$ dephosphorylation.

To determine whether the effects on protein synthesis were global or selective, and the candidate mechanisms involved, we performed low pass ribosome footprinting in C643 cells to identify subsets of mRNAs that were translated with greater (TE-high) or lesser (TE-low) efficiency than its isogenic splice reversed control (Supplementary Table S1 and S2). Interestingly *ATF4*, a known translationally regulated gene, scored as a preferentially translated candidate ( $\log_2FC:0.71$ ;  $p\text{-val}:0.005$ ;  $p\text{-adj}: 0.09$ ) (Supplementary Table S1). Accordingly, polysome profiling by density gradient fractionation showed that ATF4 mRNA was enriched in actively translating polysome fractions of NthyOri cells expressing EIF1AX-splice (Supplementary Fig. S4A). Additionally, GSEA of RNAseq of CAL62-splice vs. CAL62 cells found an ATF4 activation signature (NES:1.7; Nom p-val:0.012) (Supplementary Table S3). ATF4 is a key transcription factor that integrates responses to cell stressors, such as amino acid deficiency or ER protein folding defects. Despite the increase in ATF4, expression of the EIF1AX-splice variants was not associated with significant activation of the ER stress pathway (Supplementary Fig. S4B). *ATF4* mRNA contains two upstream open reading frames (uORF) that determine the efficiency of its translation (27). The second uORF (uORF2) overlaps with the canonical ATF4 start codon and is a strong inhibitor of ATF4 translation. Under normal conditions, translation starts at uORF1, and the ribosome dissociates at the stop codon. It reassembles at uORF2, which prevents ATF4 translation. During cellular stress, EIF2 $\alpha$  is phosphorylated at serine 51 by stress-sensing kinases. As a result, it remains GDP-bound, dampening formation of the TC (EIF2 $\alpha$  -GTP-Met-tRNA). When TC availability is limited, the ribosome fails to reassemble at uORF2, and instead reinitiates translation at the canonical ATF4 start codon (28). As EIF1AX is known to impact the fidelity of start codon selection (25,29), we tested whether EIF1AX-splice preferentially translates ATF4 by altering selectivity towards the two upstream ( $-^3ACCAUG/-^3GCCAUG$ ) and the main ( $-^3AACAUG$ ) ATF4 start codons. For this we engineered reporter constructs in which the firefly luciferase protein was under control of the different ATF4 translation initiation contexts (Kozak + start codons). Expression of EIF1AX-WT or EIF1AX-c'spl in HEK293T cells co-transfected with appropriate reporters showed that the inhibitory uORF2 led to less efficient translation in EIF1AX mutant-expressing cells (Supplementary Fig. S4C). This would conceivably de-repress translation initiation at the ATF4 mORF. Interestingly, reporter activity under control of the ATF4 mORF was also markedly increased in EIF1AX-c'spl cells (Supplementary Fig. S4C). As a complementary strategy, we used a Translation Control Reporter System (TCRS) (30) to test whether increased efficiency of ribosomal re-initiation might explain the effects of the mutant EIF1AX on ATF4 translation. Similar to ATF4, the TCRS construct has 3 ORF's: a short uORF, followed by 2 overlapping ORFs encoding a long peptide (L.P) and a short peptide (S.P), respectively, the latter serving as a marker for ribosome re-initiation (Supplementary Fig. 4D). Expression of EIF1AX NTT or c'spl mutants in HEK293T cells co-transfected with TCRS showed higher S.P levels as compared to EIF1AX-WT, indicative of higher efficiency of ribosome re-initiation. ATF4 is believed to feed forward to induce expression of its own transcript (31). Consistent with this, ATF4 mRNA was induced by ~ 3-fold in all EIF1AX-splice isogenic contexts (Supplementary Fig. S4E). The coordinate



robust increase of ATF4 gene expression may have dampened the sensitivity of the ribosome profiling experiments.

Serine 51 phosphorylation of EIF2 $\alpha$  in response to cellular stress represses global translation, but increases translational efficiency of ATF4 (27). Therefore, under physiological conditions ATF4 is downstream of p-EIF2 $\alpha$ . By contrast, EIF2 $\alpha$  in EIF1AX-splice mutant cells is paradoxically underphosphorylated. Hence, EIF1AX-splice co-opts this pathway by constitutively activating expression of ATF4, placing it upstream of EIF2 $\alpha$ , increasing availability of the ternary complex and de-repressing global translation (Fig. 4A). This is consistent with ATF4 dephosphorylating pS51-EIF2 $\alpha$  through a negative feedback loop engaged via ATF4-dependent upregulation of GADD34 (Fig. 4B), a EIF2 $\alpha$  specific cofactor for protein phosphatase-1 (PP1) (32). Moreover, the GADD34/PP1 phosphatase inhibitor salubrinal blocked EIF2 $\alpha$  dephosphorylation and preferentially repressed global protein synthesis in EIF1AX-splice vs splice-reverted C643 cells (Fig. 4C).

### EIF1AX activates mTOR through aberrant expression of ATF4 and c-MYC

We performed Gene Set Enrichment Analysis (GSEA) to identify the oncogenic signaling pathways activated by EIF1AX-splice. In addition to ATF4, the top-ranked signatures enriched in EIF1AX-mutant cells in the RNAseq profiles of the isogenic CAL62 and C643 models included the following terms: translation, ternary and 43S complex formation, mTORC1 signaling and transcriptional targets of c-MYC (Fig. 5A; Supplementary Table S3 and S4). Accordingly, the mTOR substrates P70-S6 kinase and 4EBP1 were activated by expression of the EIF1AX-splice products in both RAS-WT and RAS mutant cell lines (Fig. 5B). The EIF1AX mutant induction of mTOR signaling was not associated with PI3K pathway activation in RAS-WT cells, whereas AKT and PRAS40 phosphorylation were increased in RAS-mutant cells. Despite this, the activation of mTOR by the aberrant EIF1AX gene products was neither PI3K- nor RSK-dependent, as treatment with the pan-PI3K inhibitor GDC0941, the pan-AKT kinase inhibitor MK-2206 or the pan-RSK inhibitor LJ308 did not impair the induction of p4EBP1 in the parental C643 compared to splice-reverted cells (Supplementary Fig. S5A and S5B).

Based on these findings, we hypothesized that c-MYC and ATF4 could be key oncogenic clients of EIF1AX. Accordingly, c-MYC and ATF4 protein levels were higher in the isogenic lines and in NthyOri cells expressing the EIF1AX splice variants (Fig. 4B), as well as in mice with dox-inducible thyroid-specific expression of EIF1AX-c'spl (Fig. 5C). The increase in ATF4 and c-MYC was associated with greater abundance of aminoacid (AA) transporters for glutamine (ASCT2) and leucine (LAT1), which are known to be regulated by these transcription factors (33,34) (Fig. 4B). The differential expression of these transporters in RAS mutant thyroid cancer cell lines with endogenous *EIF1AX* mutations compared to those that were *EIF1AX*WT was particularly striking (Supplementary Fig. S5C).

We next explored whether ATF4 and/or c-MYC accounted for the increased expression of the aminoacid transporters in cells expressing EIF1AX-splice. Silencing of ATF4 or c-MYC alone modestly decreased ASCT2 abundance in C643 cells, with minimal effects on LAT1. However combined ATF4/c-MYC knockdown repressed both transporters, and decreased

p4EBP1 (Fig. 5D). This was also the case in NthyOri-splice cells (Fig. 5E). The increased expression of ASCT2 and LAT1 in EIF1AX-splice expressing cells could induce mTOR activation through increased influx of glutamine and leucine (34,35). Consistent with this, addition of leucine and glutamine in combination after 3h of aminoacid depletion resulted in a more rapid and robust induction of p4EBP1 in C643 cells compared to their isogenic wild-type revertants (Fig. 5F). The mTOR pathway in EIF1AX-splice cells was also more sensitive to depletion of glutamine (Supplementary Fig. S5D).

### ***EIF1AX* and RAS mutants converge to stabilize c-MYC, promote mTOR activation and sensitize cells to mTOR, BRD4 and MEK inhibitors.**

Deregulated expression of c-MYC in cancer is commonly due to increased protein stability. Indeed, the higher c-MYC protein levels in EIF1AX-splice expressing cells not associated with induction of c-MYC mRNA (Fig. 6A) or increased translational efficiency (Supplementary Fig. S6A). Instead, expression of EIF1AX-splice in KRAS<sup>G12R</sup>-CAL62 shifted the half-life of c-MYC from 25 to 60 min as compared to the isogenic parental cells (Fig. 6B). Silencing of oncogenic KRAS also decreased c-MYC protein levels (Fig. 6C), although to a lesser extent than in EIF1AX-splice cells, consistent with the latter cooperating with oncogenic RAS to further stabilize the protein. The key contribution of RAS and MAPK signaling to c-MYC levels was further confirmed in HTH83 cells, which harbor endogenous *HRAS*<sup>Q61R</sup> and *EIF1AX-A113splice* mutations. In these cells HRAS silencing or MEK inhibition decreased c-MYC and ASCT2 expression, whereas the pan-PI3K inhibitor GDC-0941 was without effect (Supplementary Fig. S6B and S6C).

To explore potential therapeutic dependencies of *RAS* + *EIF1AX* mutant thyroid cancers, we investigated the effects of the MEK inhibitor trametinib, the mTOR kinase inhibitor AZD8055 or the BRD4 inhibitor JQ1 (to target c-MYC transcription, with the caveat that JQ1 also inhibits other bromodomain proteins) alone and in various combinations in xenografts of CAL62-splice and parental cells. CAL62-splice xenografts grew to a larger size and were more sensitive to the growth inhibitory effects of AZD8055 or JQ1 than the parental controls, whereas trametinib had equivalent efficacy in both contexts (Fig. 6D; i, ii & iii). The combination of AZD8055 with either trametinib or JQ1 induced tumor shrinkage in CAL62-splice but not in parental cells, and was superior to either drug alone (Fig. 6D; iv, v & vi). Consistent with their effects on growth, Western blots of tumor lysates from mice treated with each condition showed that AZD8055 in combination with either trametinib or JQ1 showed the most profound inhibition of c-MYC and mTOR substrates (Fig. 6E). However, despite comparable inhibition of these signaling nodes in EIF1AX WT and mutant cells, the latter show preferential tumor shrinkage, consistent with heightened dependency on the pathways activated by these mutant proteins.

## **Discussion**

*EIF1AX* is the only PIC component that is recurrently mutated in cancers (4,5,8,21,22). *EIF1AX* mutations have been presumed to result in a change- or gain-of-function because of their predilection for specific substitutions in the N- and C-terminal tails. However, functional insights so far have been primarily confined to how *EIF1AX* mutants alter usage



of initiation codons with varying contexts in yeast (25,29). In uveal melanomas, *EIF1AX-NTT* mutants are associated with relatively indolent disease. Isolated *EIF1AX* mutations are also found in low-risk thyroid tumors (4,17). When coupled to *RAS* mutations they mark aggressive and often lethal forms of PDTC and ATC. This is phenocopied in the mouse models we described here. However, the penetrance of these cancers in *EIF1AX-c'spl/Hras<sup>G12V</sup>* mice was relatively low, suggesting that other factors may be required for transformation. In that respect, most human *EIF1AX/RAS* PDTCs and ATCs harbored either *TERT* promoter or *TP53* mutations, which are major drivers of tumor progression in this disease (5,6,36).

Phosphorylation of Ser51 of the  $\alpha$  subunit of EIF2 is a central common conduit for many cellular stress pathways, including nutrient/amino acid starvation, ER stress and oxidative insults. This modification of EIF2 $\alpha$  prevents its recycling into the TC, thereby inhibiting global protein synthesis, which helps cells to adapt by conserving nutrients and relieving ER stress. However, a subset of mRNAs, most prominently ATF4, are preferentially translated. ATF4 induces a transcriptional program that includes genes involved in amino acid transport, metabolism and protection from oxidative stress, which allow cells to orchestrate a more sustained adaptation to these stressors (37–43). The induction of ATF4 in *EIF1AX-A113splice* cells is independent of EIF2 $\alpha$  phosphorylation, and takes place by modulating ATF4 translation efficiency as well as inducing its transcription. This illegitimate ATF4 activation then hijacks a negative feedback pathway that leads to dephosphorylation of Ser51 of EIF2 $\alpha$ , by inducing expression of GADD34, a co-factor for the EIF2 $\alpha$  phosphatase PP1 (32,43), thus increasing global protein synthesis. Hence, this mutated translation initiation component attains a gain-of-function by deregulating the stringent control of the rate of global protein synthesis by EIF2 $\alpha$  dephosphorylation. This in itself has significant oncogenic potential, as expression of hypo-phosphorylated EIF2 $\alpha$  is sufficient to transform NIH3T3 cells (44).

*RAS* mutations are found along the entire spectrum of thyroid cancer, although the frequency is markedly enriched in PDTC and ATC (5). Allelic imbalance favoring oncogenic *Ras* gene dosage appears to be critical for transformation, and can be achieved through loss of the WT copy (45) or mutant allele amplification (46–48). Intensification of *RAS* signaling in thyroid cancer can also be mediated through YAP-induced transcriptional activation of *RAS*, leading to tumor progression (26). Oncogenic *RAS* acts via ERK to prevent c-MYC degradation, primarily through phosphorylation of serine 62, a site within the c-MYC degron recognized by a specific E3 ubiquitin ligase (49,50). pS62-c-MYC primes subsequent phosphorylation at threonine 58, which facilitates dephosphorylation of S62, poisoning MYC for degradation. We found that *EIF1AX-splice* increased c-MYC protein half-life, further augmenting the effects of oncogenic *RAS* signaling on c-MYC protein stability. Interestingly, transcription-independent MYC-MAX activation was seen in the uveal melanoma (UM) TCGA study in the context of *EIF1AX-NTT* mutations (16). Consistent with this, the *EIF1AX* mutations in uveal melanoma display mutual exclusivity to tumors with chromosome 8q gain, which harbors the *MYC* gene locus (8q<sup>24.21</sup>). Conceivably, by analogy to the *RAS-EIF1AX* cooperativity on MYC in thyroid cancer, a potential mechanistic basis of MYC-MAX activation in uveal melanomas may involve

interactions with constitutive G-protein oncogenic signaling mediated by the co-occurring *GNAQ/GNA11* mutations in *EIF1AX*-mutant uveal melanomas (8,16).

The intersection of ATF4 and c-MYC on regulation of amino acid transporter expression and mTOR activation is well established (33–35). We found that c-MYC and ATF4 co-regulated amino acid transporters in the *EIF1AX*-RAS context, particularly ASCT2 and LAT1, leading to mTOR activation. Accordingly, expression of ATF4, c-MYC and amino acid transporters in a panel of RAS-mutant human thyroid cancer cell lines displayed a striking concordance with *EIF1AX* mutation. These events cooperate to sensitize mTOR signaling to amino acid supply. *EIF1AX*-splice also slightly augments RAS-induced PI3K signaling in the isogenic cell lines, through unclear mechanisms. However, the activation of mTOR is PI3K-AKT- and RSK-independent, and driven primarily by the increased influx of amino acids. Whether increased PI3K contributions to tumorigenesis through alternative mechanisms in this context cannot be ruled out.

In summary, *EIF1AX-A113splice*, a mutation commonly encountered in thyroid cancer in association with oncogenic *RAS*, leads to induction of ATF4, which in turn induces a global increase in protein synthesis through GADD34-dependent dephosphorylation of EIF2 $\alpha$ . The mutant *EIF1AX*, in concert with oncogenic *RAS*, also increases c-MYC protein stability. c-MYC and ATF4 cooperate to induce transcription of amino acid transporters, and the resulting amino acid flux activates mTOR signaling. Our data point to mTOR kinase as a primary node for pharmacological targeting, and provides a rationale for MEK or c-MYC co-inhibition to maximize therapeutic responses (Fig. 7).

Besides the ~ 11% of advanced thyroid cancers harboring *EIF1AX* and *RAS* mutations, these two oncogenes also co-occur in low grade serous ovarian cancers (21) and in some widely invasive Hurthle cell carcinomas. mTOR kinase inhibitors are currently not approved for any indication. However, they are still being extensively investigated in combination with other agents. The findings reported here provide a strong rationale for combined mTOR and MEK inhibitors for tumors harboring these defects.

## Methods and Materials

### Cell lines.

Cell lines were maintained at 37°C and 5% CO<sub>2</sub> in humidified atmosphere and were grown in RPMI-1640 for Nthy-Ori 3–1, C643, CAL62 and HTH83, DMEM for HEK293T, HTH7, ACT1 and DMEM:RPMI for KMH2 supplemented with 10% of FBS, 2 mmol/l glutamine, 50 U/mL penicillin (GIBCO), and 50  $\mu$ g/mL streptomycin. C643, Hth7 and Hth83 cell lines were obtained from Dr. Nils-Erik Heldin, Uppsala University Hospital, Sweden. CAL62 cells were obtained from Dr. Jeanine Gioanni, Centre Antoine-Lacassagne, France. The ACT1 line was obtained from Dr. Naoyoshi Onoda, Osaka City University Graduate School of Medicine, Japan. KMH2 were obtained from Japanese Collection of Research Bioresources Cell Bank (JCRB), Japan. All cell lines tested negative for mycoplasma and were authenticated using short tandem repeat and single nucleotide polymorphism analyses.

### Plasmids and constructs.

The cDNAs of the EIF1AX splice variants (c'spl and t'spl) were cloned by PCR amplification from parental *EIF1AX-A113splice* mutant human thyroid cell line HTH83. The full-length cDNAs of human wild type EIF1AX and the EIF1AX splice variants (c'spl and t'spl) were cloned into pLVX-puro and the dox-inducible pLVX-Tight-puro vectors (Clontech). EIF1AX N-terminal tail (NTT) mutants were generated from pLVX-puro-EIF1AX-WT by site-directed mutagenesis (Stratagene protocol). The EIF1AX c'spl cDNA was cloned into the pLVX-puro vector or the pLVX-Tight-puro vector. Bicistronic expression constructs for EIF1AX-WT and the two EIF1AX splice variants were generated by sequential cloning into pLVX-Tight-puro, as schematically shown in Supplementary Fig. S2C. The PCR primers used to amplify EIF1AX-WT, to generate NTT mutants by site-directed mutagenesis, or to amplify the specific splice variants in cell lines harboring endogenous *EIF1AX* mutations are shown in Supplementary Table S5. The TCRS and the TCRS<sup>uORF</sup> vector systems were provided by Dr. Cor Calkhoven (ERIBA, Groningen, NL). The targeting plasmid ColA1-TRE (ColA-CHC system for cDNA expression) used to clone the EIF1AX-c'spl cDNA was provided by Dr. Luke Dow (Weill Cornell College of Medicine, NY). All constructs were sequence-verified.

### Development of isogenic EIF1AX-splice-expressing and EIF1AX-splice-repaired thyroid cancer cell lines by CRISPR-Cas9.

CAL62 and TTA1 cells, which are WT for *EIF1AX*, were modified to endogenously express EIF1AX splice variants (cryptic and truncated splice) by targeted disruption of the splice acceptor site by CRISPR-Cas9. A 20bp CRISPR guide sequence (sgRNA) was designed to span the splice site of exon 6, exploiting the endogenous PAM sequence within the splice acceptor site (Supplementary Table S5). The sgRNA was annealed and cloned into the pLentiCRISPR vector (Addgene # 49535) that transcribes Cas9 and the CRISPR guide/tracer RNA. Parental CAL62 and TTA1 cells were transfected with pLentiCRISPR-SgRNA using FuGENE HD, followed by selection in 1 µg/mL puromycin for 3 days. Cells were then grown for 5 to 7 days, and then plated as single cells into 96-well plates. The propagated clones were tested for disruption of the EIF1AX exon 6 splice site by PCR-based sequencing of genomic DNA encompassing the targeted region. The substitutions introduced in CAL62 and TTA1 cells effectively disrupted the splice acceptor site but were not identical to the naturally occurring endogenous *EIF1AX-A113spl* mutations. Positive clones of CAL62-splice and TTA1-splice were confirmed for expression of EIF1AX c'splice and t'splice mRNAs and their encoded proteins by immunoblotting.

The parental C643 cell line, which harbors an endogenous *EIF1AX-A113splice* mutation, was used to revert the mutant allele by CRISPR-Cas9 knock-in of the corresponding WT sequence through use of a homologous directed repair template (HDR). The sgRNA targeting intron 5 was cloned into the pX330 vector (Addgene# 42230). The homologous recombination donor vector was designed using vector builder (<https://www.vectorbuilder.com/design.html>). Specifically, the donor vector (Vector ID: VB160426-1022eqv) was designed to integrate into the intron 5 locus upon recombination directed by homologous arms of 629bp (right) and 701bp (left) flanking a puromycin resistance cassette. The two arms encompassed the 3' end of intron5, the entire exon6 and a fragment of intron6.

C643 cells were co-transfected with pX330-sgRNA and the donor vector harboring the HDR template. After 72h cells were subjected to puromycin selection. Surviving cells were seeded as single cells in a 96-well plate for testing. Clones that were positive for the targeted locus by PCR-based sequencing were tested for expression of the splice variant mRNAs by RT-PCR and by immunoblotting. Clone C643-spl-rev (C643-Xcl18) was used in this manuscript.

### EIF1AX overexpression in cell lines.

Nthy-Ori 3–1 cells (hereafter referred to as NthyOri, derived from wild-type human thyroid cells immortalized with large T-antigen) (51) were used to generate stable and dox-inducible lines expressing EIF1AX-WT, NTT-mutants or the splice variants. The pLVX-puro vector cloned with the respective various EIF1AX cDNA's were used for constitutive expression, whereas the pLVX-Tet-On Advanced vector system (Clontech) was used to generate dox-inducible EIF1AX or bicistronically expressed EIF1AX-splice variants, as described in 'Plasmids and Constructs' section.

To generate stable EIF1AX-expressing NthyOri clones, the constructs described above were used for lentiviral production in HEK293FT cells using the Mission Lentiviral Packing Mix (SIGMA). The constitutively expressing NthyOri-EIF1AX stable lines were generated by infecting with the corresponding viral particles, and the dox-inducible NthyOri-EIF1AX cells by co-infecting with lentiviral-transduced pLVX-Tight-puro-EIF1AX and pLVX-Tet-On particles in the presence of 8 µg/mL polybrene (Sigma, St Louis, MO) overnight. After 24 hours in complete medium, cells were selected in 1 µg/mL puromycin with or without 300 µg/ml G418 as required. The mass culture was then cloned into single cells, which were expanded and tested for the expression or induction of EIF1AX by immunoblotting.

### Tg-rtTA/TRE-EIF1AX-c'spl and TPO-Cre/FR-Hras<sup>G12V</sup> mice.

The dox-inducible *EIF1AX-c'spl* mouse model was developed by the ESC-GEMM method (52). ESC derived from *TPO-Cre/FR-Hras<sup>het</sup>/RIK<sup>het</sup>/CHC<sup>het</sup>* mice were used to target the human EIF1AX-c'spl cDNA into the homing cassette that directs site-specific integration of the transgene downstream of the *Col1a1* locus by recombination-mediated cassette exchange. The *TPO-Cre* drives Cre recombinase under the control of the thyroid peroxidase gene promoter, which is active in thyroid cells at E14.5 (53). ESC clones targeted with *TRE-EIF1AX-c'spl* into the *Col1a1*-homing cassette (CHC) were microinjected into blastocysts produced from NCI C57BL/6-cBrd/cBrd/Cr (C57BL/6 albino) mice and implanted into CD-1 pseudo-pregnant mothers enabling production of chimeric pups. To achieve higher expression of rtTA we bred out the *RIK<sup>het</sup>* cassette and bred in thyroglobulin-driven rtTA (*Tg-rtTA(s)M2*) (54). The resulting *TPO-Cre/FR-Hras<sup>het</sup>/Tg-rtTA/TRE-EIF1AX<sup>het</sup>* mice were intercrossed to generate the following lines: *TPO-Cre/FR-Hras<sup>hom</sup>,Tg-rtTA/TRE-EIF1AX<sup>hom</sup>* and *TPO-Cre/FR-Hras<sup>hom</sup>/Tg-rtTA/TRE-EIF1AX<sup>hom</sup>*. All animals were fed doxycycline-impregnated chow (TD01306, Envigo), and the appropriate lines verified by immunoblotting to achieve dox-inducible expression of EIF1AX-c'spl in thyroid follicular cells (Fig. 2C). Animal care and all procedures were approved by the MSKCC Institutional Animal Care and Use Committee.

### Histology and Immunohistochemistry.

Mouse thyroids dissected from surrounding tissues were fixed in 4% paraformaldehyde, embedded in paraffin, sectioned and stained with hematoxylin and eosin (H&E). Histological diagnosis was performed by a thyroid pathologist (RG) blinded to mouse genotype. Sections were also immunostained for KI67. Slides were scanned with Panoramic Flash 250 (3DHistech, Budapest, Hungary), and whole thyroid lobes or regions of interest viewed using Panoramic Viewer and exported as tiff images. H&E and IHC were performed by the MSK Molecular Cytology Core Facility.

### Western Blotting and Immunoprecipitation.

Cells were lysed in 1X RIPA buffer (Millipore) supplemented with protease (Roche) and phosphatase inhibitor cocktails I & II (Sigma). Tumors or xenografts were homogenized in 1X Lysis Buffer (containing 10 mmol Tris-HCl, 5 mmol EDTA, 4 mmol EGTA, 1% Triton-X100) with protease/phosphatase inhibitors. Lysates were briefly sonicated to disrupt the tissue and cleared by centrifugation. Protein concentrations were estimated by BCA kit (Thermo Scientific) on a microplate reader (SpectraMax M5); comparable amounts of proteins were subjected to SDS page using NuPAGE 4–12% Bis-Tris gradient gels (Invitrogen) and were then transferred to PVDF membranes. Following overnight primary antibody incubation, membranes were incubated with secondary antibodies coupled to horseradish peroxidase (HRP) or IRDye fluorophores for 1h at room temperature. HRP probed blots were developed using enhanced chemiluminescence reagent (Amersham Biosciences), and signal captured using X-ray films or with the KwikQuant™ Imager (<http://kindlebio.com/index.php>). IRDye-probed blots were imaged using the LICOR Odyssey imaging system (Licor Biosciences). Immunoblot quantification was done using ImageJ.

For co-immunoprecipitation experiments, cells were lysed in buffer containing 75 mM NaCl, 50 mM Hepes, 10 mM MgCl<sub>2</sub>, 8 mM EGTA, 10 mM β-glycerophosphate, 1 mM DTT, 0.5% Triton X-100, along with protease and phosphatase inhibitors. Equal amounts of lysate (500μg) were diluted with lysis buffer in 300μl final volume; 1/10<sup>th</sup> of the volume was denatured and used as input control. Antibodies were incubated with lysates overnight by end-to-end rotation at 4 °C. Antigen-antibody complexes were immobilized by incubating with Dyna beads for 1h, the antibody-antigen-beads collected by DynaMag™-spin (Invitrogen), washed with lysis buffer, denatured and subjected to Western blotting.

### Antibodies.

The following primary antibodies were used for immunoblots at a dilution of 1:1000, except where indicated. EIF1AY (sc-84243) was used to immunoblot EIF1AX, EIF5 (sc-28309), EIF2α (sc-11386), HRAS (sc-520; 1:500), KRAS (sc-30; 1:500), YB1 (sc-101198), HA-tag (sc-805) were obtained from Santa Cruz biotechnology. c-MYC (5605), ATF4 (11815), LAT1 (5347), ASCT2 (5100), pEIF2α-S51 (9721), pAKT-S473 (4051), pAKT-T308 (4056), AKT (2920), pP70S6K-T389 (9234), P70S6K (2708), p4EBP1-S65 (9451), p4EBP1-T37/46 (2855), 4EBP1 (9452), pYB1-S102 (2900), pRPS6-S240/244 (2215), pRPS6-S235/236 (2211), RPS6 (2317), pERK (9101), ERK (4696), HA-Tag (3724), Biotin (5597), ER stress antibody sampler kit (9956) were from Cell Signaling, pPRAS40-T246 (441100G),

GADD34 (PA1–139) from Invitrogen, ASCT2 (HPA035240) and  $\beta$ -actin (A2228; 1: 10000) from Sigma Aldrich.

The secondary antibodies were used at a dilution of 1:5000. HRP-conjugated antibodies included goat anti-rabbit (Santa Cruz; sc-2004) and goat anti-mouse (Santa Cruz; sc-2031). IRDye fluorophore-conjugated antibodies were IRDye® 800CW Goat anti-Rabbit IgG (Licor; 926–32211), IRDye® 800CW Goat anti-Mouse IgG (Licor; 926–32210), IRDye® 680RD Goat anti-Rabbit IgG (Licor; 926–68071), and IRDye® 680RD Goat anti-Mouse IgG (Licor; 926–68070). We also used the following additional reagents: Doxycycline (2  $\mu$ g/mL) and cycloheximide were from Sigma. Salubrinal was from Calbiochem. LJI308 was from Selleckchem.

### **L-azidohomoalanine (AHA) labeling.**

Isogenic cell lines used to assess nascent protein synthetic rate were grown in 60-mm dishes until ~70% confluent. Prior to labeling cells were incubated with methionine-free media containing 2% FBS for 1h, followed by addition of 50  $\mu$ M AHA (Life Technologies, C10102) for 20min. Cells were then washed in cold PBS and immediately lysed in buffer containing 50 mM Tris HCl, pH 8.0, and 1% SDS. Complete lysis was achieved by sonication. Comparable amounts of lysates were then subjected to Click-iT reaction for switching azido-modified nascent proteins to alkyne-biotin (Life Technologies, B10185) using the Click-iT™ Protein Reaction Buffer Kit (Life Technologies, C10276) following the manufacturer's protocol. Biotinylated nascent proteins were subjected to immunoblotting using either anti-biotin, EIF1AX or  $\beta$ -actin primary antibodies and the corresponding IRDye-fluorophore-conjugated secondary antibodies. Images were captured by the LICOR Odyssey imaging system. Biotinylated proteins on the entire lane was quantified using Odyssey application software version 3.0 (LICOR Biosciences).

### **RNA interference.**

We used SMARTpools (Dharmacon) for ATF4 and c-MYC silencing (Dharmacon). Cells grown without antibiotics at 70% confluence were transfected using 50 nmol/L of Smartpools and 6–8  $\mu$ L of DharmaFECT (Dharmacon). SiRNAs for HRAS and KRAS were from ORIGENE and were transfected using SiTran1.0 as per manufacturer's instructions. Cells were harvested 72h post-transfection and analyzed by Western blotting.

### **RNA isolation, cDNA synthesis and qPCR.**

Total RNA from isogenic cell lines was extracted using the PrepEase Kit (USB Corporation). Comparable amounts of RNA (1 $\mu$ g) were subjected to DNase I (Invitrogen) treatment and reverse transcribed using SuperScript® III Reverse Transcriptase (Invitrogen) following the manufacturer's protocol. qPCR was then performed with the Power SYBR Green PCR Master Mix (Applied Biosystems). Primers used are shown in Supplementary Table S5. The Ct values of the target genes were normalized to  $\beta$  actin and the normalized expression analyzed by the Ct method.



**c-MYC half-life.**

The relative half-life of c-MYC protein in CAL62 vs. CAL62-splice cells was analyzed by measuring c-MYC protein abundance after treatment with cycloheximide (CHX). Cells plated in 60-mm dishes and grown 24h in low serum condition (0.5% FBS) were treated with 100 µg/ml cycloheximide (Sigma), harvested and lysed at the indicated time points and analyzed by Western blotting.

**Colony formation assay.**

Dishes were first coated with a bottom layer of 0.4% agar in RPMI. Cells were resuspended in a top layer of 0.2% agar in RPMI with 10% FBS, and then fed every other day by adding drops of media onto the top layer. After 3 weeks, the colonies were stained with crystal violet and counted in a GelCount™ colony counter (Oxford OPTRONIX). Minimum diameter of the colonies was set to 100µm.

**Tumor xenografts.**

Approximately 6–8 week-old female SCID mice (NOD.CB17-Prkdc; Envigo RMS.Inc) were injected subcutaneously with  $5 \times 10^6$  CAL62 or CAL62-splice cells grown to 70% confluence and resuspended in 50% Matrigel (CORNING) into the right and left flanks, respectively. Treatments were administered by oral gavage when tumor volume approached  $200 \text{ mm}^3$  as estimated by measuring the length and width with calipers ( $\text{width}^2 \times \text{length} \times 0.52$ ). Tumor-bearing mice were randomly assigned into 5 treatment arms: Controls (vehicle-4% DMSO in 30% PEG 300); AZD8055 (10 mg/kg); Trametinib (0.75 mg/kg); JQ1 (40 mg/kg); AZD8055 + Trametinib and AZD8055 + JQ1 (all drugs were from Selleckchem). Mice were weighed at the start of treatment and every second day during the treatment period. AZD8055 was dissolved in a mixture of 4% DMSO and 30% PEG 300 (SIGMA), trametinib in 4% DMSO in corn oil and JQ1 in 2% DMSO, 30% PEG 300 and 5% Tween 80. Treatments were administered by oral gavage in a volume of approximately 200 µL. Tumor volume was measured every 2–3 days with calipers. After 21 days mice were humanely killed, and dissected tumors flash frozen for subsequent protein isolation. All animal experiments were performed in accordance with a protocol approved by the Institutional Animal Care and Use of Committee (IACUC) of Memorial Sloan Kettering Cancer Center.

**Statistical analyses.**

Statistical analysis for animal studies and cell lines was performed using GraphPad Prism 7. P value was determined by two-tailed t-tests. F test was used to compare variances between the groups, if different, Welch correction was applied. Data are shown as mean with SD or mean with 95% CI (n=3 or more biological replicates).

**Translation Efficiency Analysis by Ribosome profiling.**

Ribosome profiling and RNA seq were performed in C643 and C643-spl-rev cells. Triplicates of cells grown in 150mm dishes were treated with cycloheximide for 10 min and ribosome-protected RNA fragments isolated following the published protocol for ribosome profiling (55) with a modification of including unique molecular identities (UMI) in the

library reverse transcription primer (Supplementary Table S5) in order to remove PCR duplicates during analysis. Parallel total RNA extraction was performed for RNA-seq. Ribosome profiling reads and RNA-Seq reads were aligned using STAR v2.5. (56) using the UCSC human genome reference, hg19 (<http://hgdownload.cse.ucsc.edu/goldenPath/hg19/chromosomes>) with ERCC spike-ins included as an extra chromosome. To process the ribosome profiling reads before alignment, linker sequences (5'-CTGTAGGCACCATCAAT-3') were removed using Trimmomatic v0.32 (57) with the following parameters: number of mismatches between read and adapter: 2; length of alignment between read and adapter: 6. Clipped reads were then filtered to be a minimum length of 25. Reads with unique molecular identifiers (5'-NNNNTGANNNNCC-3') were removed from the sequence and inserted into the read name using UMI tools v2.1.1 (58). The set parameters for STAR during alignment were as follows: each read must uniquely map; number of mismatches: 2; maximum intron alignment length: 500000; 3' adapter sequence: CTGTAGGCAC; maximum proportion of mismatches within adapter: 0.1; default values were used for all remaining parameters:

```
STAR --runThreadN 4 --genomeLoad NoSharedMemory --outSAMtype BAM
Unsorted --outSAMstrandField intronMotif --outSAMattributes NH HI NM MD
AS XS --outSAMunmapped Within --outSAMheaderHD @HD VN:1.4 --
outFilterMultimapNmax 0 --outFilterMultimapScoreRange 1 --
outFilterScoreMinOverLread 0.33 --outFilterMatchNminOverLread 0.33 --
outFilterMismatchNmax 2 --alignIntronMax 500000 --alignMatesGapMax
1000000 --alignSJDBoverhangMin 1 --sjdbOverhang 100 --sjdbScore 2 --
readFilesCommand zcat --clip3pAdapterSeq CTGTAGGCAC --
clip3pAdapterMMp 0.1
```

Read alignments are available on NCBI SRA under accession number SRP142722. To remove possible rRNA contamination, both the ribosome profiling and RNA-Seq reads were aligned to ribosomal sequences gathered from BioMart Ensembl (59) and SILVA (60) databases and merged into a single FASTA reference file (GEO accession GSE113695). Reads were again aligned using STAR with almost all the same parameters, but reads were allowed to align to a maximum of 3 other regions in our rRNA FASTA reference. All reads which aligned to the rRNA reference according to the criteria above were filtered from the original genome reference aligned reads:

```
STAR --runThreadN 4 --genomeLoad NoSharedMemory --outSAMtype BAM
Unsorted --outSAMstrandField intronMotif --outSAMattributes NH HI NM MD
AS XS --outSAMunmapped Within --outSAMheaderHD @HD VN:1.4 --
outFilterMultimapNmax 3 --outFilterMultimapScoreRange 1 --
outFilterScoreMinOverLread 0.33 --outFilterMatchNminOverLread 0.33 --
outFilterMismatchNmax 2 --alignIntronMax 500000 --alignMatesGapMax
1000000 --alignSJDBoverhangMin 1 --sjdbOverhang 100 --sjdbScore 2 --
readFilesCommand zcat --clip3pAdapterSeq CTGTAGGCAC --
clip3pAdapterMMp 0.1
```

For final filtering, all ribosomal reads larger than 35 base pairs were removed and all reads aligning to the same position with the same UMI were reduced to a single read using UMI

tools. The final alignment files used for quantifications are available on GEO accession GSE113695.

To estimate abundance on the aligned BAM files, a custom script was used with gencode annotation version 19 and additional ERCC spike-in sequences (ERCC92). For RNA-Seq samples with spike-ins, the library size normalization factor was estimated using DESeq2 v3.6 (61). The library size normalization was used in the differential translation efficiency analysis. RiboDiff v0.2.1 (62) with default parameters was used to estimate the change in translational efficiency between sample conditions. Only protein coding genes (Gencode v19) were considered in RiboDiff. The result of RiboDiff is available in the Supplementary Table S1 and S2. We used the following command line: `ribodiff -p 1 -s 10 -m BH`

### **Polysome Fractionation.**

NthyOri-splice dox-inducible cells were treated with or without dox for 72 h, followed by cycloheximide (100 $\mu$ g/ml) for 15 min. Cells were then trypsinized and lysed with buffer containing 15mM Tris-HCl, 300mM NaCl, 15mM MgCl<sub>2</sub>, 1% Triton X-100, 0.1mg/ml cycloheximide and ribonuclease inhibitor (RNasin, PROMEGA). Comparable amounts of lysates (1.5 mg protein) were then layered onto a 10–60% sucrose density gradient prepared in 15mM Tris-HCl, 300mM NaCl, 15mM MgCl<sub>2</sub>, 0.1mg/ml cycloheximide and RNasin, and fractionated using a SW60Ti rotor in a Beckman ultracentrifuge for 2 h at 37,000 rpm at 4°C. After centrifugation, the gradients were collected manually from the top into 12 fractions. Fractions were subjected to RNA extraction for ATF4, c-MYC and  $\beta$ -actin mRNA measurements by real time PCR as described (63).

### **RNAseq-Gene Set Enrichment Analysis (GSEA).**

Gene set enrichment analysis (64) was performed with GSEA software (<http://www.broadinstitute.org/gsea/>) using the pre-defined Canonical Pathways and Hallmarks Molecular Signatures Database (MSigDB) gene sets (<http://software.broadinstitute.org/gsea/msigdb/index.jsp>). The normalized counts of each replicate (GEO accession GSE113695) derived from the RNA-seq of C643 vs C643-spl-rev and CAL62-splice vs CA62 cells were used as a dataset to run GSEA analysis (Identification-Gene symbol; permutations-1000 and permutation type-gene sets). Briefly, GSEA software-derived enrichment scores (ES) identified the functional group of genes (pre-defined datasets in the MsigDB) over-represented in the given data set. The Normalized Enrichment Score (NES) was used to determine statistical significance from the nominal p value after controlling for false positives by calculating false discovery rate (FDR). Key top-ranked signatures based on NES, Nom-p-value and FDR-q value prompted validation in our experimental models.

### **Luciferase and TCRS assay.**

The pGL3-firefly vector was engineered with the ATF4 uORF initiation context by site directed mutagenesis (primers shown in Supplementary Table S5). HEK293T cells were co-transfected with EIF1AX-WT, G9R or c'splice expression vectors along with the engineered firefly vectors using Fugene HD. Renilla luciferase (pRL-null) was co-transfected as a transfection efficiency control. Cells were incubated in 0.5% FBS for 48h and luciferase

activity measured using the Dual-Glo Luciferase Assay system on the GloMax-Multi Microplate Reader (Promega).

The efficiency of a ribosomal re-initiation mode of translation in EIF1AX-WT and the mutants was assessed with the translation control reporter system (TCRS) as described previously (30). The TCRS construct has a short uORF and 2 overlapping ORFs encoding a long peptide (L.P) and a short peptide (S.P), respectively, the latter being a marker of ribosomal re-initiation. HEK293T cells co-transfected with TCRS and EIF1AX-WT, -NTT mutants or EIF1AX-c'spl expression vectors. The expression of the short peptide was analyzed by immunoblotting.

## Supplementary Material

Refer to Web version on PubMed Central for supplementary material.

## Acknowledgements:

Supported by NIH P50-CA72012, RO1-CA72597 and RO1-CA50706 (J.A.F.), R01-CA204228 (S.D.L), U54 OD020355-01 (S.W.L) and by P30-CA008748, We thank the MSKCC Research Animal Resource Center and the following core labs for their support: Molecular Cytology, Pathology and the Integrative Genomics Operation funded by Cycle for Survival and the Marie-Josée and Henry R. Kravis Center for Molecular Oncology. We are also grateful to Dr. Cor Calkhoven (ERIBA, NL) for helpful advice and reagents.

## References

1. Kimura ET, Nikiforova MN, Zhu Z, Knauf JA, Nikiforov YE, Fagin JA. High prevalence of BRAF mutations in thyroid cancer: genetic evidence for constitutive activation of the RET/PTC-RAS-BRAF signaling pathway in papillary thyroid carcinoma. *Cancer Res* 2003;63(7):1454–7. [PubMed: 12670889]
2. Ciampi R, Knauf JA, Kerler R, Gandhi M, Zhu Z, Nikiforova MN, et al. Oncogenic AKAP9-BRAF fusion is a novel mechanism of MAPK pathway activation in thyroid cancer. *J Clin Invest* 2005;115(1):94–101 doi 10.1172/JCI23237. [PubMed: 15630448]
3. Ricarte-Filho JC, Li S, Garcia-Rendueles ME, Montero-Conde C, Voza F, Knauf JA, et al. Identification of kinase fusion oncogenes in post-Chernobyl radiation-induced thyroid cancers. *J Clin Invest* 2013;123(11):4935–44 doi 10.1172/JCI69766. [PubMed: 24135138]
4. Cancer Genome Atlas Research N. Integrated genomic characterization of papillary thyroid carcinoma. *Cell* 2014;159(3):676–90 doi 10.1016/j.cell.2014.09.050. [PubMed: 25417114]
5. Landa I, Ibrahimasic T, Boucai L, Sinha R, Knauf JA, Shah RH, et al. Genomic and transcriptomic hallmarks of poorly differentiated and anaplastic thyroid cancers. *J Clin Invest* 2016;126(3):1052–66 doi 10.1172/JCI85271. [PubMed: 26878173]
6. Pozdeyev N, Gay LM, Sokol ES, Hartmaier R, Deaver KE, Davis S, et al. Genetic Analysis of 779 Advanced Differentiated and Anaplastic Thyroid Cancers. *Clin Cancer Res* 2018 doi 10.1158/1078-0432.CCR-18-0373.
7. Kunstman JW, Juhlin CC, Goh G, Brown TC, Stenman A, Healy JM, et al. Characterization of the mutational landscape of anaplastic thyroid cancer via whole-exome sequencing. *Hum Mol Genet* 2015;24(8):2318–29 doi 10.1093/hmg/ddu749. [PubMed: 25576899]
8. Martin M, Masshofer L, Temming P, Rahmann S, Metz C, Bornfeld N, et al. Exome sequencing identifies recurrent somatic mutations in EIF1AX and SF3B1 in uveal melanoma with disomy 3. *Nat Genet* 2013;45(8):933–6 doi 10.1038/ng.2674. [PubMed: 23793026]
9. Sharp AJ, Stathaki E, Migliavacca E, Brahmachary M, Montgomery SB, Dupre Y, et al. DNA methylation profiles of human active and inactive X chromosomes. *Genome Res* 2011;21(10):1592–600 doi 10.1101/gr.112680.110. [PubMed: 21862626]

10. Pestova TV, Borukhov SI, Hellen CU. Eukaryotic ribosomes require initiation factors 1 and 1A to locate initiation codons. *Nature* 1998;394(6696):854–9 doi 10.1038/29703. [PubMed: 9732867]
11. Kozak M The scanning model for translation: an update. *J Cell Biol* 1989;108(2):229–41. [PubMed: 2645293]
12. Hinnebusch AG. Molecular mechanism of scanning and start codon selection in eukaryotes. *Microbiol Mol Biol Rev* 2011;75(3):434–67, first page of table of contents doi 10.1128/MMBR.00008-11. [PubMed: 21885680]
13. Jones RM, Branda J, Johnston KA, Polymenis M, Gadd M, Rustgi A, et al. An essential E box in the promoter of the gene encoding the mRNA cap-binding protein (eukaryotic initiation factor 4E) is a target for activation by c-myc. *Mol Cell Biol* 1996;16(9):4754–64. [PubMed: 8756633]
14. Fernandez PC, Frank SR, Wang L, Schroeder M, Liu S, Greene J, et al. Genomic targets of the human c-Myc protein. *Genes Dev* 2003;17(9):1115–29 doi 10.1101/gad.1067003. [PubMed: 12695333]
15. Truitt ML, Conn CS, Shi Z, Pang X, Tokuyasu T, Coody AM, et al. Differential Requirements for eIF4E Dose in Normal Development and Cancer. *Cell* 2015;162(1):59–71 doi 10.1016/j.cell.2015.05.049. [PubMed: 26095252]
16. Robertson AG, Shih J, Yau C, Gibb EA, Oba J, Mungall KL, et al. Integrative Analysis Identifies Four Molecular and Clinical Subsets in Uveal Melanoma. *Cancer Cell* 2017;32(2):204–20 e15 doi 10.1016/j.ccell.2017.07.003. [PubMed: 28810145]
17. Karunamurthy A, Panebianco F, S JH, Vorhauer J, Nikiforova MN, Chiosea S, et al. Prevalence and phenotypic correlations of EIF1AX mutations in thyroid nodules. *Endocr Relat Cancer* 2016;23(4):295–301 doi 10.1530/ERC-16-0043. [PubMed: 26911375]
18. Nicolson NG, Murtha TD, Dong W, Paulsson JO, Choi J, Barbieri AL, et al. Comprehensive Genetic Analysis of Follicular Thyroid Carcinoma Predicts Prognosis Independent of Histology. *J Clin Endocrinol Metab* 2018 doi 10.1210/jc.2018-00277.
19. Sette M, van Tilborg P, Spurio R, Kaptein R, Paci M, Gualerzi CO, et al. The structure of the translational initiation factor IF1 from E.coli contains an oligomer-binding motif. *EMBO J* 1997;16(6):1436–43 doi 10.1093/emboj/16.6.1436. [PubMed: 9135158]
20. Battiste JL, Pestova TV, Hellen CU, Wagner G. The eIF1A solution structure reveals a large RNA-binding surface important for scanning function. *Mol Cell* 2000;5(1):109–19. [PubMed: 10678173]
21. Etemadmoghadam D, Azar WJ, Lei Y, Moujaber T, Garsed DW, Kennedy CJ, et al. EIF1AX and NRAS Mutations Co-occur and Cooperate in Low-Grade Serous Ovarian Carcinomas. *Cancer Res* 2017;77(16):4268–78 doi 10.1158/0008-5472.CAN-16-2224. [PubMed: 28646021]
22. Cancer Genome Atlas Research N, Brat DJ, Verhaak RG, Aldape KD, Yung WK, Salama SR, et al. Comprehensive, Integrative Genomic Analysis of Diffuse Lower-Grade Gliomas. *N Engl J Med* 2015;372(26):2481–98 doi 10.1056/NEJMoa1402121. [PubMed: 26061751]
23. Fekete CA, Applefield DJ, Blakely SA, Shirokikh N, Pestova T, Lorsch JR, et al. The eIF1A C-terminal domain promotes initiation complex assembly, scanning and AUG selection in vivo. *EMBO J* 2005;24(20):3588–601 doi 10.1038/sj.emboj.7600821. [PubMed: 16193068]
24. Fekete CA, Mitchell SF, Cherkasova VA, Applefield D, Algire MA, Maag D, et al. N- and C-terminal residues of eIF1A have opposing effects on the fidelity of start codon selection. *EMBO J* 2007;26(6):1602–14 doi 10.1038/sj.emboj.7601613. [PubMed: 17332751]
25. Martin-Marcos P, Zhou F, Karunasiri C, Zhang F, Dong J, Nanda J, et al. eIF1A residues implicated in cancer stabilize translation preinitiation complexes and favor suboptimal initiation sites in yeast. *Elife* 2017;6 doi 10.7554/eLife.31250.26.
26. Garcia-Rendueles ME, Ricarte-Filho JC, Untch BR, Landa I, Knauf JA, Voza F, et al. NF2 Loss Promotes Oncogenic RAS-Induced Thyroid Cancers via YAP-Dependent Transactivation of RAS Proteins and Sensitizes Them to MEK Inhibition. *Cancer Discov* 2015;5(11):1178–93 doi 10.1158/2159-8290.CD-15-0330 [PubMed: 26359368]
27. Vattem KM, Wek RC. Reinitiation involving upstream ORFs regulates ATF4 mRNA translation in mammalian cells. *Proc Natl Acad Sci U S A* 2004;101(31):11269–74 doi 10.1073/pnas.0400541101. [PubMed: 15277680]

28. B'Chir W, Maurin AC, Carraro V, Averous J, Jousse C, Muranishi Y, et al. The eIF2alpha/ATF4 pathway is essential for stress-induced autophagy gene expression. *Nucleic Acids Res* 2013;41(16):7683–99 doi 10.1093/nar/gkt563. [PubMed: 23804767]
29. Saini AK, Nanda JS, Lorsch JR, Hinnebusch AG. Regulatory elements in eIF1A control the fidelity of start codon selection by modulating tRNA(i)(Met) binding to the ribosome. *Genes Dev* 2010;24(1):97–110 doi 10.1101/gad.1871910. [PubMed: 20048003]
30. Wiesenthal V, Leutz A, Calkhoven CF. A translation control reporter system (TCRS) for the analysis of translationally controlled processes in the vertebrate cell. *Nucleic Acids Res* 2006;34(3):e23 doi 10.1093/nar/gnj029. [PubMed: 16473846]
31. Kilberg MS, Pan YX, Chen H, Leung-Pineda V. Nutritional control of gene expression: how mammalian cells respond to amino acid limitation. *Annu Rev Nutr* 2005;25:59–85 doi 10.1146/annurev.nutr.24.012003.132145. [PubMed: 16011459]
32. Ma Y, Hendershot LM. Delineation of a negative feedback regulatory loop that controls protein translation during endoplasmic reticulum stress. *J Biol Chem* 2003;278(37):34864–73 doi 10.1074/jbc.M301107200. [PubMed: 12840028]
33. Wise DR, DeBerardinis RJ, Mancuso A, Sayed N, Zhang XY, Pfeiffer HK, et al. Myc regulates a transcriptional program that stimulates mitochondrial glutaminolysis and leads to glutamine addiction. *Proc Natl Acad Sci U S A* 2008;105(48):18782–7 doi 10.1073/pnas.0810199105. [PubMed: 19033189]
34. Chen R, Zou Y, Mao D, Sun D, Gao G, Shi J, et al. The general amino acid control pathway regulates mTOR and autophagy during serum/glutamine starvation. *J Cell Biol* 2014;206(2):173–82 doi 10.1083/jcb.201403009. [PubMed: 25049270]
35. Wang Q, Holst J. L-type amino acid transport and cancer: targeting the mTORC1 pathway to inhibit neoplasia. *Am J Cancer Res* 2015;5(4):1281–94. [PubMed: 26101697]
36. Liu X, Bishop J, Shan Y, Pai S, Liu D, Murugan AK, et al. Highly prevalent TERT promoter mutations in aggressive thyroid cancers. *Endocr Relat Cancer* 2013;20(4):603–10 doi 10.1530/ERC-13-0210. [PubMed: 23766237]
37. Wek RC, Jiang HY, Anthony TG. Coping with stress: eIF2 kinases and translational control. *Biochem Soc Trans* 2006;34(Pt 1):7–11 doi 10.1042/BST20060007. [PubMed: 16246168]
38. Wortel IMN, van der Meer LT, Kilberg MS, van Leeuwen FN. Surviving Stress: Modulation of ATF4-Mediated Stress Responses in Normal and Malignant Cells. *Trends Endocrinol Metab* 2017;28(11):794–806 doi 10.1016/j.tem.2017.07.003. [PubMed: 28797581]
39. Chevet E, Hetz C, Samali A. Endoplasmic reticulum stress-activated cell reprogramming in oncogenesis. *Cancer Discov* 2015;5(6):586–97 doi 10.1158/2159-8290.CD-14-1490. [PubMed: 25977222]
40. Hanahan D, Weinberg RA. Hallmarks of cancer: the next generation. *Cell* 2011;144(5):646–74 doi 10.1016/j.cell.2011.02.013. [PubMed: 21376230]
41. Feng YX, Sokol ES, Del Vecchio CA, Sanduja S, Claessen JH, Proia TA, et al. Epithelial-to-mesenchymal transition activates PERK-eIF2alpha and sensitizes cells to endoplasmic reticulum stress. *Cancer Discov* 2014;4(6):702–15 doi 10.1158/2159-8290.CD-13-0945. [PubMed: 24705811]
42. Harding HP, Zhang Y, Zeng H, Novoa I, Lu PD, Calfon M, et al. An integrated stress response regulates amino acid metabolism and resistance to oxidative stress. *Mol Cell* 2003;11(3):619–33. [PubMed: 12667446]
43. Novoa I, Zhang Y, Zeng H, Jungreis R, Harding HP, Ron D. Stress-induced gene expression requires programmed recovery from translational repression. *EMBO J* 2003;22(5):1180–7 doi 10.1093/emboj/cdg112. [PubMed: 12606582]
44. Donze O, Jagus R, Koromilas AE, Hershey JW, Sonenberg N. Abrogation of translation initiation factor eIF-2 phosphorylation causes malignant transformation of NIH 3T3 cells. *EMBO J* 1995;14(15):3828–34. [PubMed: 7641700]
45. Bremner R, Balmain A. Genetic changes in skin tumor progression: correlation between presence of a mutant ras gene and loss of heterozygosity on mouse chromosome 7. *Cell* 1990;61(3):407–17. [PubMed: 2185890]



46. Finney RE, Bishop JM. Predisposition to neoplastic transformation caused by gene replacement of H-ras1. *Science* 1993;260(5113):1524–7. [PubMed: 8502998]
47. Namba H, Gutman RA, Matsuo K, Alvarez A, Fagin JA. H-ras protooncogene mutations in human thyroid neoplasms. *J Clin Endocrinol Metab* 1990;71(1):223–9 doi 10.1210/jcem-71-1-223. [PubMed: 2196280]
48. Chen X, Mitsutake N, LaPerle K, Akeno N, Zanzonico P, Longo VA, et al. Endogenous expression of Hras(G12V) induces developmental defects and neoplasms with copy number imbalances of the oncogene. *Proc Natl Acad Sci U S A* 2009;106(19):7979–84 doi 10.1073/pnas.0900343106. [PubMed: 19416908]
49. Farrell AS, Sears RC. MYC degradation. *Cold Spring Harb Perspect Med* 2014;4(3) doi 10.1101/cshperspect.a014365.
50. Hayes TK, Neel NF, Hu C, Gautam P, Chenard M, Long B, et al. Long-Term ERK Inhibition in KRAS-Mutant Pancreatic Cancer Is Associated with MYC Degradation and Senescence-like Growth Suppression. *Cancer Cell* 2016;29(1):75–89 doi 10.1016/j.ccell.2015.11.011. [PubMed: 26725216]
51. Lemoine NR, Mayall ES, Jones T, Sheer D, McDermid S, Kendall-Taylor P, et al. Characterisation of human thyroid epithelial cells immortalised in vitro by simian virus 40 DNA transfection. *Br J Cancer* 1989;60(6):897–903. [PubMed: 2557880]
52. Premsrirut PK, Dow LE, Kim SY, Camiolo M, Malone CD, Miething C, et al. A rapid and scalable system for studying gene function in mice using conditional RNA interference. *Cell* 2011;145(1):145–58 doi 10.1016/j.cell.2011.03.012. [PubMed: 21458673]
53. Kusakabe T, Kawaguchi A, Kawaguchi R, Feigenbaum L, Kimura S. Thyrocyte-specific expression of Cre recombinase in transgenic mice. *Genesis* 2004;39(3):212–6 doi 10.1002/gene.20043. [PubMed: 15282748]
54. Chakravarty D, Santos E, Ryder M, Knauf JA, Liao XH, West BL, et al. Small-molecule MAPK inhibitors restore radioiodine incorporation in mouse thyroid cancers with conditional BRAF activation. *J Clin Invest* 2011;121(12):4700–11 doi 10.1172/JCI46382. [PubMed: 22105174]
55. Ingolia NT, Brar GA, Rouskin S, McGeachy AM, Weissman JS. The ribosome profiling strategy for monitoring translation in vivo by deep sequencing of ribosome-protected mRNA fragments. *Nat Protoc* 2012;7(8):1534–50 doi 10.1038/nprot.2012.086. [PubMed: 22836135]
56. Dobin A, Davis CA, Schlesinger F, Drenkow J, Zaleski C, Jha S, et al. STAR: ultrafast universal RNA-seq aligner. *Bioinformatics* 2013;29(1):15–21 doi 10.1093/bioinformatics/bts635. [PubMed: 23104886]
57. Bolger AM, Lohse M, Usadel B. Trimmomatic: a flexible trimmer for Illumina sequence data. *Bioinformatics* 2014;30(15):2114–20 doi 10.1093/bioinformatics/btu170. [PubMed: 24695404]
58. Smith T, Heger A, Sudbery I. UMI-tools: modeling sequencing errors in Unique Molecular Identifiers to improve quantification accuracy. *Genome Res* 2017;27(3):491–9 doi 10.1101/gr.209601.116. [PubMed: 28100584]
59. Flicek P, Ahmed I, Amode MR, Barrell D, Beal K, Brent S, et al. Ensembl 2013. *Nucleic Acids Res* 2013;41(Database issue):D48–55 doi 10.1093/nar/gks1236. [PubMed: 23203987]
60. Quast C, Pruesse E, Yilmaz P, Gerken J, Schweer T, Yarza P, et al. The SILVA ribosomal RNA gene database project: improved data processing and web-based tools. *Nucleic Acids Res* 2013;41(Database issue):D590–6 doi 10.1093/nar/gks1219. [PubMed: 23193283]
61. Love MI, Huber W, Anders S. Moderated estimation of fold change and dispersion for RNA-seq data with DESeq2. *Genome Biol* 2014;15(12):550 doi 10.1186/s13059-014-0550-8. [PubMed: 25516281]
62. Wolfe AL, Singh K, Zhong Y, Drewe P, Rajasekhar VK, Sanghvi VR, et al. RNA G-quadruplexes cause eIF4A-dependent oncogene translation in cancer. *Nature* 2014;513(7516):65–70 doi 10.1038/nature13485. [PubMed: 25079319]
63. Panda AC, Martindale JL, Gorospe M. Polysome Fractionation to Analyze mRNA Distribution Profiles. *Bio Protoc* 2017;7(3) doi 10.21769/BioProtoc.2126.
64. Subramanian A, Tamayo P, Mootha VK, Mukherjee S, Ebert BL, Gillette MA, et al. Gene set enrichment analysis: a knowledge-based approach for interpreting genome-wide expression

profiles. Proc Natl Acad Sci U S A 2005;102(43):15545–50 doi 10.1073/pnas.0506580102.  
[PubMed: 16199517]

Author Manuscript

Author Manuscript

Author Manuscript

Author Manuscript

### Significance

Mutations of *EIF1AX*, a component of the translation preinitiation complex, co-occur with *RAS* in advanced thyroid cancers and promote tumorigenesis. *EIF1AX-A113splice* drives an ATF4-induced dephosphorylation of EIF2 $\alpha$ , resulting in increased protein synthesis. ATF4 also cooperates with c-MYC to sensitize mTOR to aminoacid supply, thus generating vulnerability to mTOR kinase inhibitors.

Author Manuscript

Author Manuscript

Author Manuscript

Author Manuscript

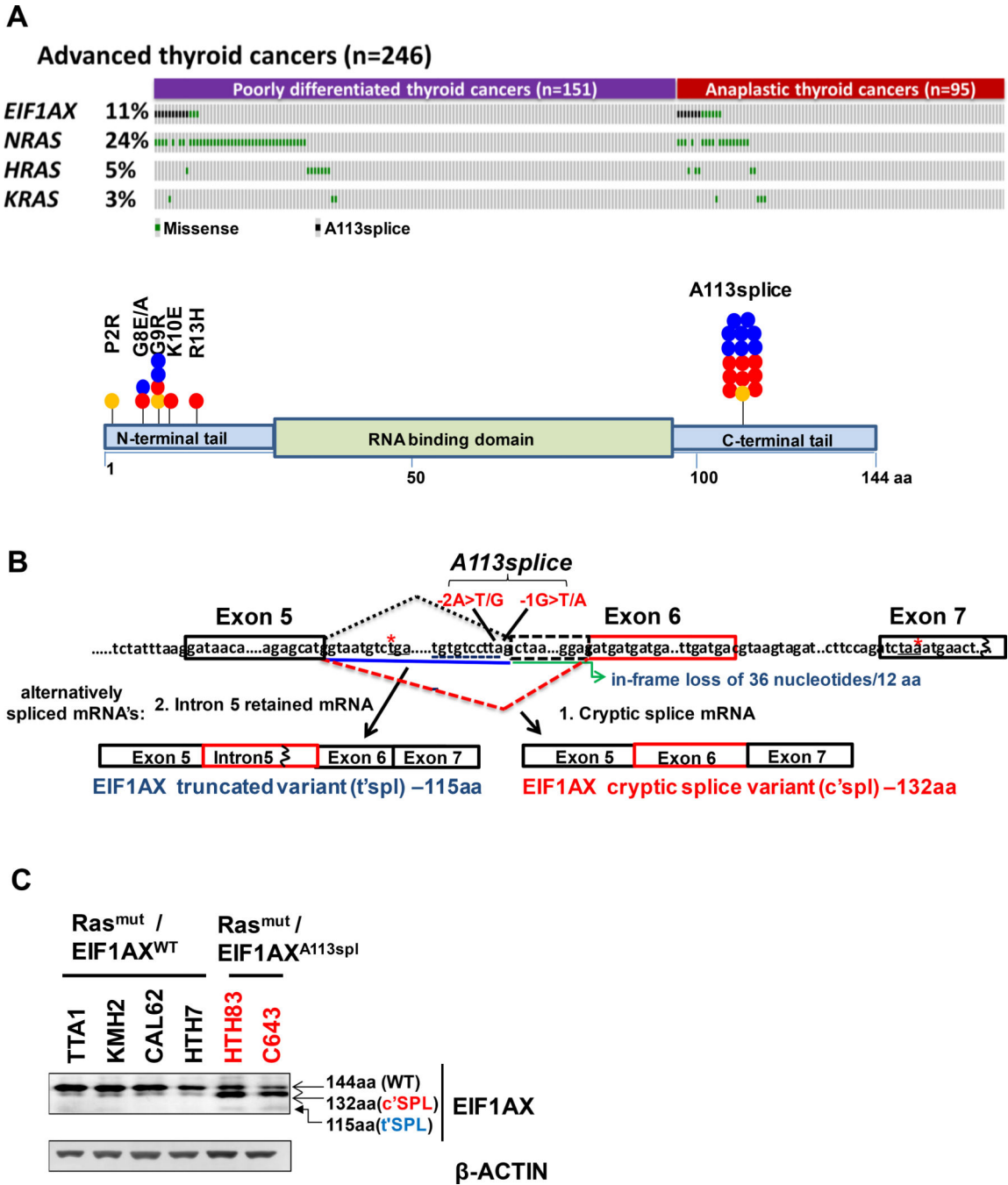


**Figure 1: EIF1AX mutation is a strong co-operating event with RAS in advanced thyroid cancer; the hotspot A113splice mutation induces aberrant splice variants.**

(A) *Top*: EIF1AX and RAS mutations in 151 PDTC and 95 ATC, compiled from MSK clinical series (n=148 as of Oct 2017), Landa *et al* (n=76) (5) and Kunstman *et al* (n=22) (7). Oncoprint shows co-occurrence of EIF1AX and RAS mutations in 25/26 tumors; p=3.15×10E-13; Fisher’s exact test. Green: EIF1AX or RAS missense mutations; Black: EIF1AX-A113splice mutation. *Bottom*: Distribution of EIF1AX mutations, showing cluster of missense mutations in the N-terminal tail and in a hotspot splice acceptor upstream of exon 6 in the C-terminal tail (red dots (MSK series); blue (5) and yellow (7)).

(B) Scheme of aberrant mRNA splicing by the *EIF1AX-A113splice* mutations c.338-1G>A/T or c.338-2A>T/G, which abolish the splice acceptor site of exon 6 (dotted line), resulting in two alternatively spliced mRNA's: 1. Cryptic splice (c'spl) mRNA, through usage of a cryptic splice acceptor site within exon 6, yielding a 132aa protein (Black dotted line: normal splice junction; red dotted line: cryptic splice junction; green arrow: position of in-frame 12aa loss). 2. Intron 5 retained mRNA: failure to splice out intron 5 (blue dotted line) yields a 115aa truncated protein (t'spl). Red asterisk points to stop codon..

(C) EIF1AX Western immunoblot of human *RAS* mutant cell lines with or without the endogenous *EIF1AX-A113splice* mutation. Arrows point to EIF1AX-wt and the mutant EIF1AX-c'spl and EIF1AX-t'spl proteins.

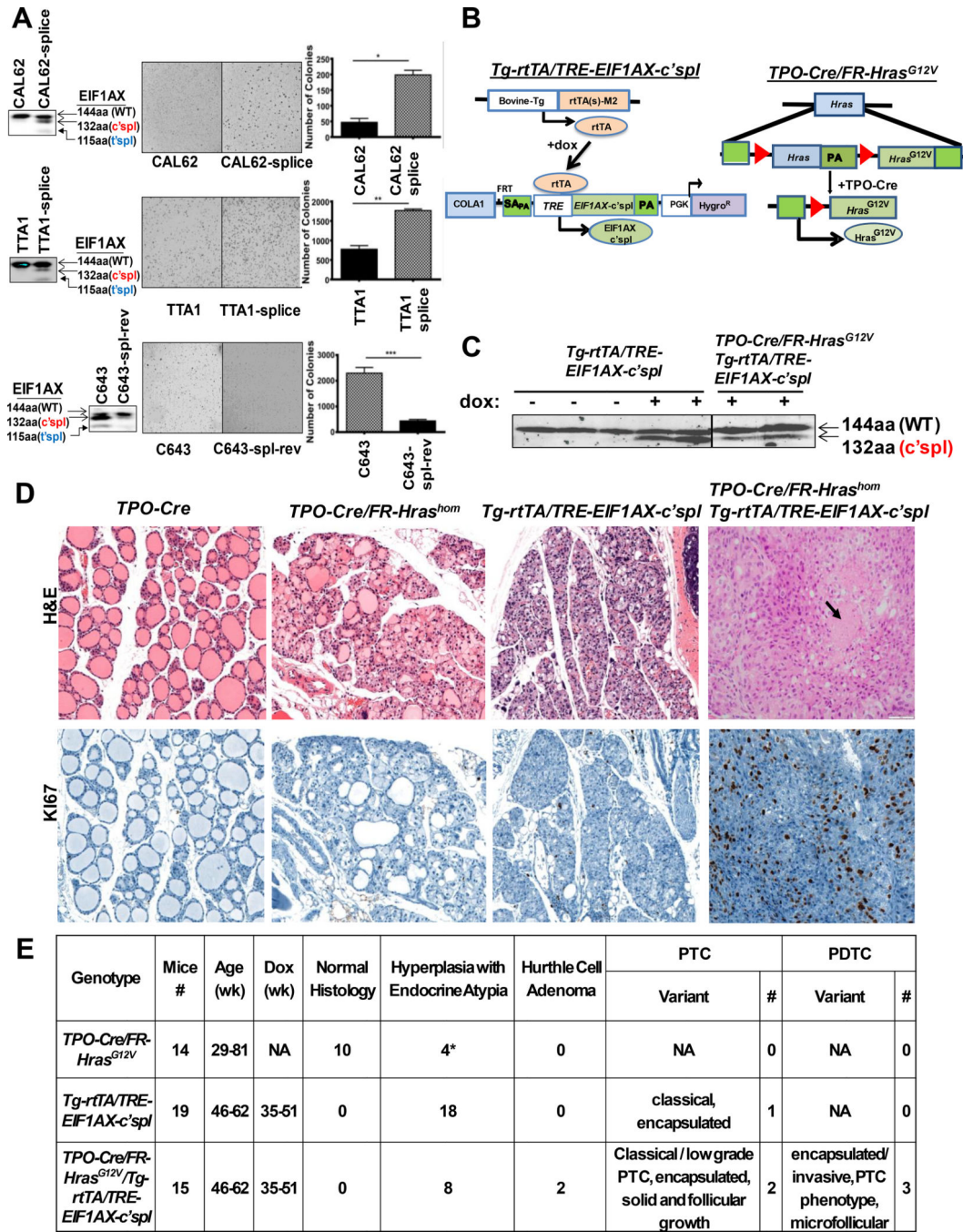


**Figure 2: Aberrant splice variants of EIF1AX-A113splice mutation induce transformation *in vitro* and cooperate with oncogenic RAS to promote mouse thyroid tumorigenesis.**

(A) *Left*: EIF1AX immunoblot of EIF1AX-A113splice knock-in cells (CAL62-splice and TTA1-splice) showing *de novo* expression of cryptic and truncated splice variants, and their loss in repaired cells (C643-spl-rev), in which the splice mutation has been reverted to WT. *Middle and right panels*: Soft agar colony assays of the corresponding isogenic cell lines in the EIF1AX-splice and EIF1AX/RAS contexts. \* $p < 0.0002$ , \*\* $p < 0.0001$ , \*\*\* $p < 0.0001$ ; two tailed unpaired t test;  $n = 3$ .



- (B) Targeting constructs used to develop *Tg-rtTA/TRE-EIF1AX-c'spl/TPO-Cre/FR-Hras<sup>G12V</sup>* mice.
- (C) EIF1AX immunoblot of lysates of mouse thyroid tissues in *Tg-rtTA/TRE-EIF1AX-c'spl* mice fed with or without dox diet for 40–51 weeks..
- (D) *Top*: Representative H&E stained thyroid sections of the indicated genotypes after 40–51 weeks of dox. Histology of mice with isolated *Hras* or *EIF1AX-c'spl* revealed hyperplasia, whereas compound *Tpo-Cre/FR-Hras<sup>G12V</sup>/Tg-rtTA/TRE-EIF1AX-c'spl* mice developed tumors consistent with PDTC; arrow pointing necrosis. *Bottom*: Corresponding KI67 IHC..
- (E) Histological characteristics of thyroid tissues from *TPO-Cre/FR-Hras<sup>G12V</sup>*, *TRE-EIF1AX-c'spl* and *TPO-Cre/FR-Hras<sup>G12V</sup>/TRE-EIF1AX-c'spl* mice. Prevalence of thyroid cancer: *EIF1AX/Hras* vs. *EIF1AX*  $p = 0.03$ ; *EIF1AX/Hras* vs *Hras*  $p = 0.01$  (unpaired t test). \*Hyperplasia of *Hras*-mutant tumors lacks atypical features, whereas in the *EIF1AX* context all hyperplastic lesions had endocrine atypia.

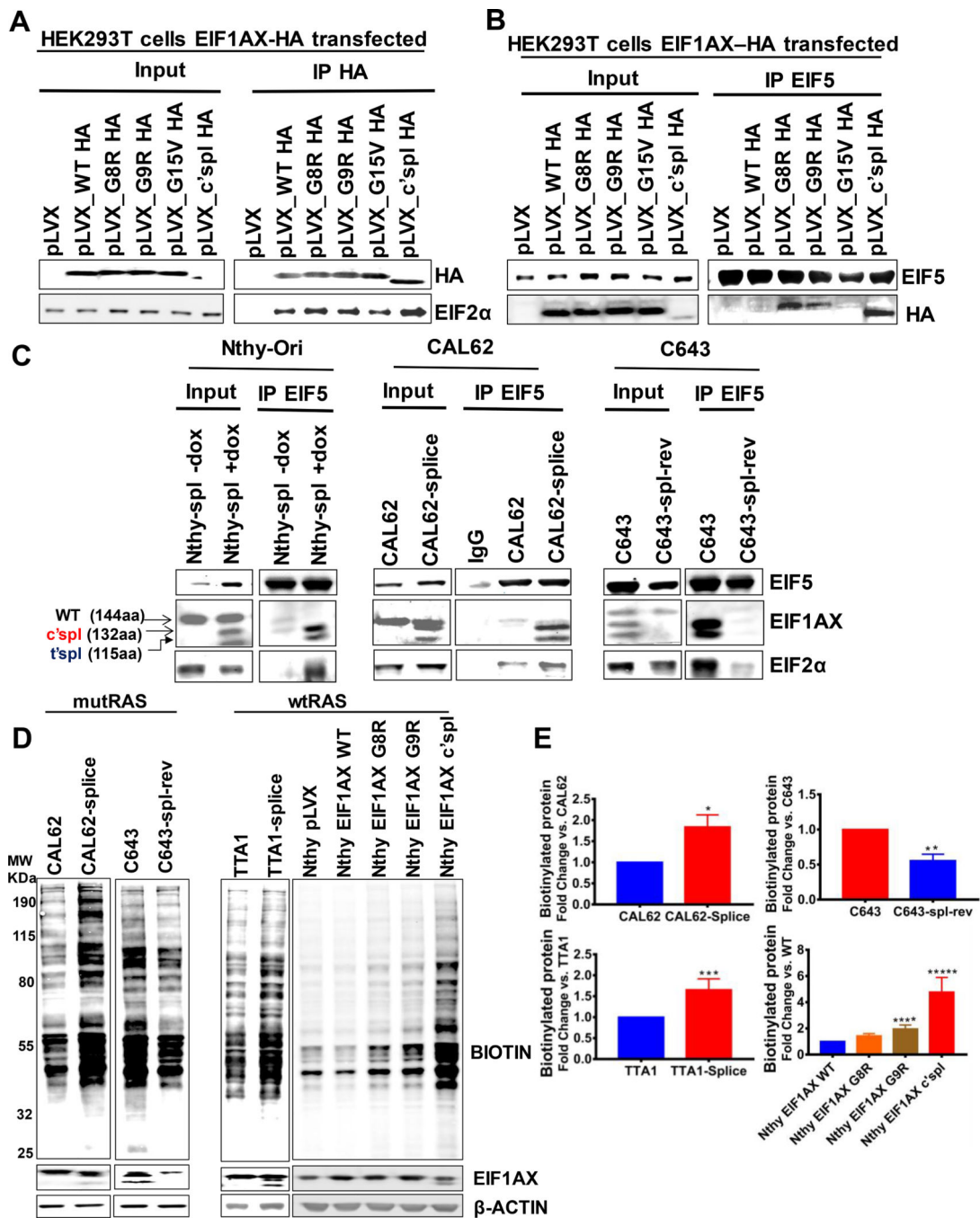


**Figure 3: EIF1AX mutants have higher affinity to components of the translation PIC and increase protein synthesis..**

(A) Input lysates (*left*) and Co-IP (*right*) of HEK293T lysates transfected with empty vector or HA-tagged EIF1AX-WT or the following EIF1AX mutants: -G8R, -G9R, -G15V or -c'spl. EIF1AX mutants efficiently co-IP the ternary complex component EIF2α.

(B) HEK293T lysates transfected with the indicated constructs showed more efficient co-IP of EIF1AX mutants vs WT-EIF1AX with an antibody to the PIC subunit EIF5. *Left*: Input lysates. *Right*: EIF5 co-IP.

(C) EIF5 co-IP of EIF1AX in the following contexts: NthyOri cells with dox-inducible expression of EIF1AX-c'splice, EIF1AX-splice knock-in (CAL62-splice) and in splice-reversed (C643-spl-rev) cells compared to their respective parental isogenic cells. Splice variants were IP more efficiently than EIF1AX-WT, which was associated with higher pull-down of the ternary complex protein EIF2 $\alpha$ . Arrows point to EIF1AX WT, -c'spl and -t'spl proteins.

(D) *De novo* protein synthesis of *EIF1AX*-splice isogenic lines (left) or NthyOri cells transfected with the indicated EIF1AX constructs (right) as determined by L-azidohomoalanine (AHA) labeling. Cells were starved of methionine for 1h and incubated with AHA for 20min. Lysates were subjected to a click-it chemistry reaction to switch azido-modified nascent proteins to alkyne-biotin, and visualized by anti-biotin immunoblotting. Bottom panel: Immunoblots for EIF1AX and  $\beta$ -actin.

(E). Quantification of biotinylated nascent protein in the indicated cells (\* $p < 0.03$ , \*\* $p < 0.002$ , \*\*\* $p < 0.015$ , \*\*\*\* $p < 0.03$ , \*\*\*\*\* $p < 0.02$ ; paired t test). Data in C, D and E are representative of three independent experiments

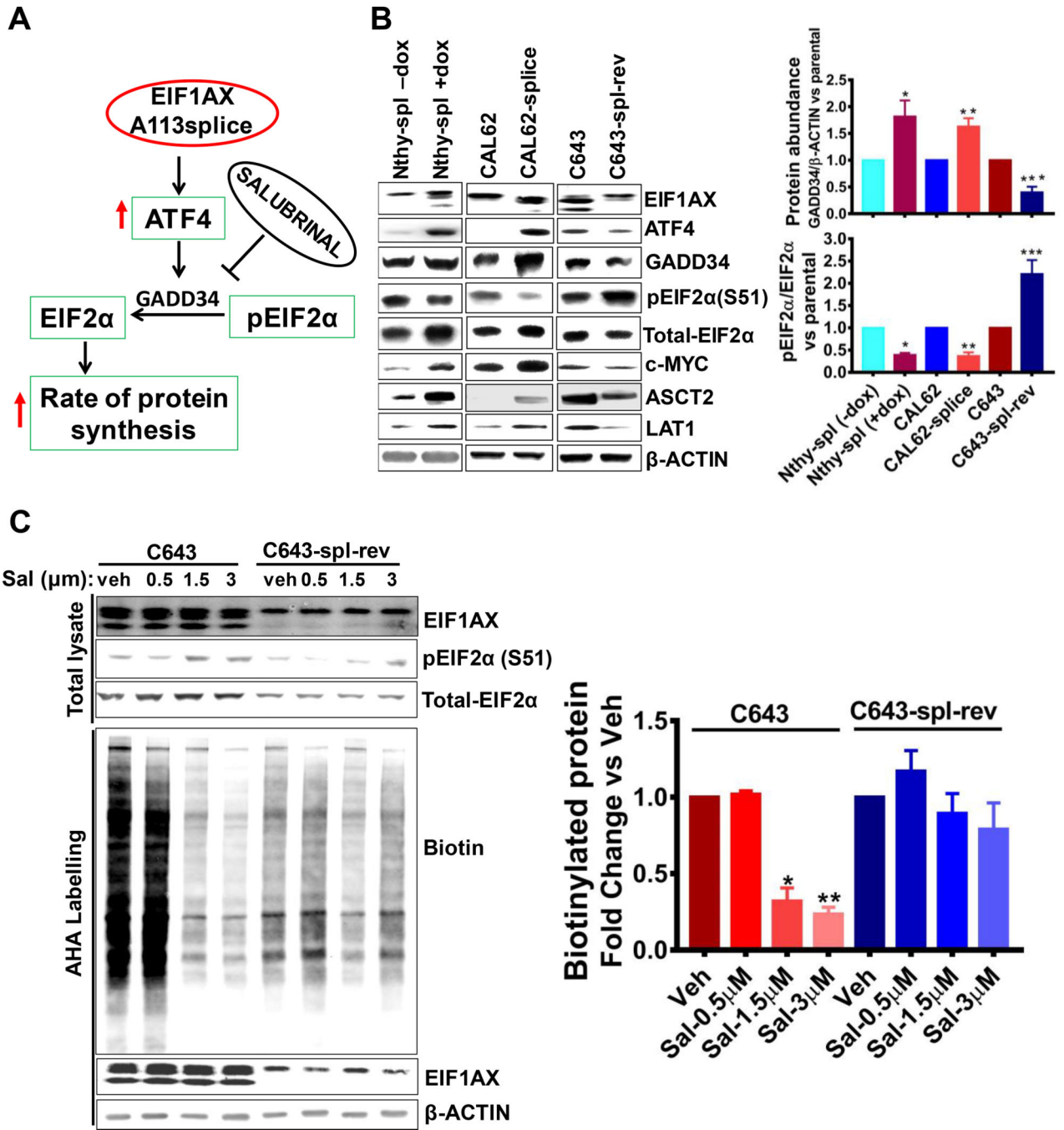


**Figure 4: Increased global protein synthesis by EIF1AX-splice is mediated by ATF4-induced EIF2α dephosphorylation..**

(A) Schematic representation of negative feedback inhibition of EIF2α phosphorylation by ATF4. ATF4 induces GADD34 mRNA, a component of the protein phosphatase 1 complex, which dephosphorylates EIF2α. Salubrinal, a selective GADD34/PP1 inhibitor, reverses this effect, leading to derepression of protein synthesis.

(B) *Left*: Western immunoblot of the indicated proteins in NthyOri-splice and *RAS/EIF1AX*-splice isogenic lines. *Right*: Quantification of GADD34/βactin and pEIF2α/tEIF2α

in EIF1AX-splice-expressing cells (GADD34: \* $p < 0.04$ , \*\* $p < 0.019$ , \*\*\* $P < 0.01$ ; EIF2 $\alpha$ : \* $p < 0.001$ , \*\* $p < 0.006$ , \*\*\* $p < 0.02$ ; paired t test).

(C) *Top*: Immunoblot for EIF1AX, total and pEIF12 $\alpha$  in vehicle or Salubrinal treated C643 and C643-spl-rev cells. *Bottom*: *De novo* protein synthesis by AHA labeling of C643 vs. C643-spl-rev cells treated with vehicle or the indicated concentration of Salubrinal. *Right*: Salubrinal attenuated protein synthetic rate in EIF1AX-splice cells (\* $p < 0.005$ , \* $p < 0.001$ ; paired t test). Data in B and C are representative of three independent experiments.

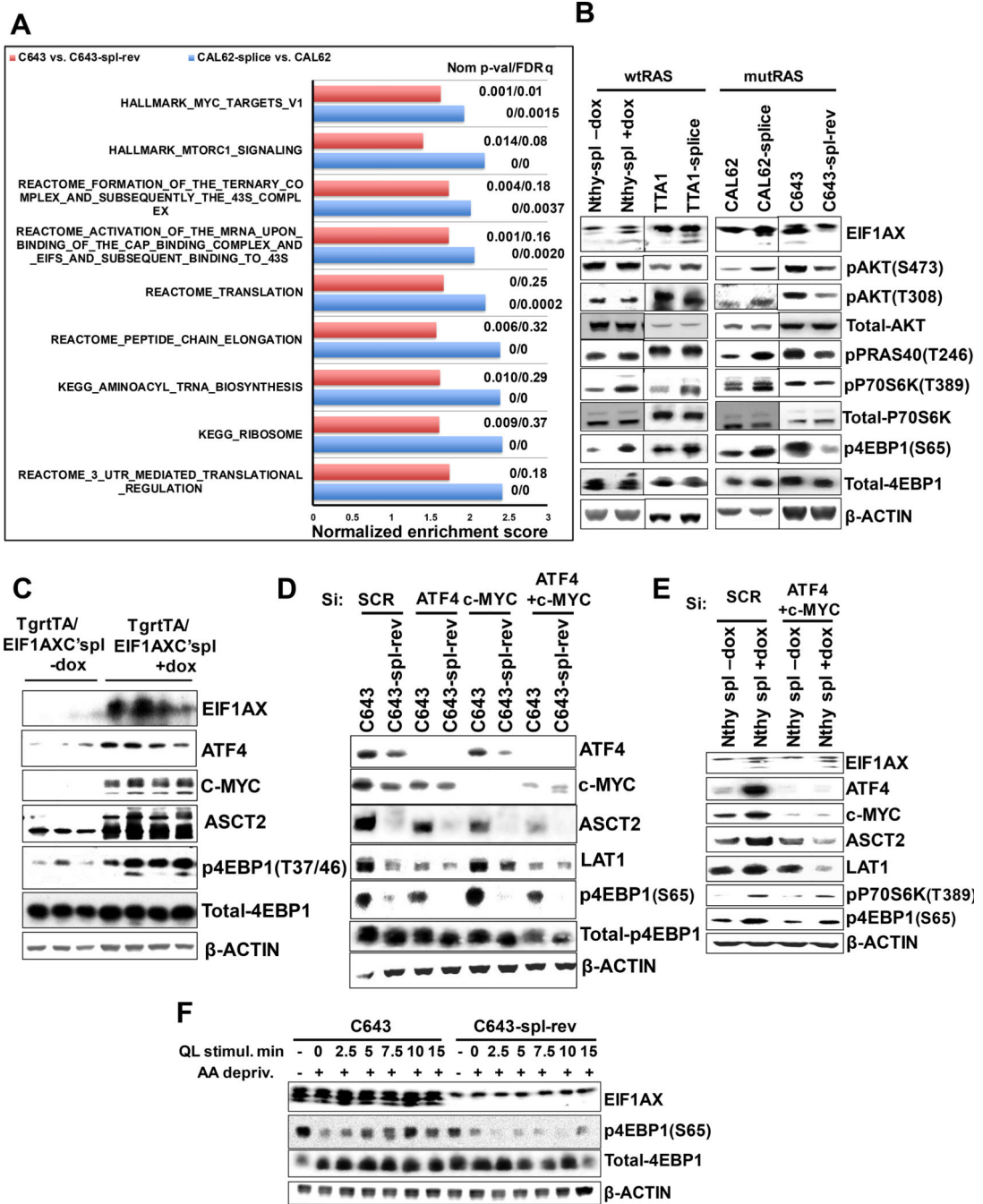


**Figure 5: EIF1AX activates mTOR through aberrant expression of ATF4 and c-MYC..**  
 (A) GSEA analysis from RNAseq of CAL62-splice and C643 compared to respective isogenic WT controls using MsigDB ‘hallmarks’ and ‘canonical pathways’ genesets showed activation of pathways associated with c-MYC, mTORC1, preinitiation complex formation, translation and tRNA aminoacylation. NES were plotted and Nom p-value/FDR q-value is indicated for each signature..



(B) Immunoblot for PI3K and mTOR substrates in the indicated isogenic thyroid cell lines modified for expression of EIF1AX-splice in RAS-WT (dox-inducible NthyOri cells, TTA1) or *RAS* mutant cells (CAL62 and C643).

(C) Western blots of thyroid tissue lysates of *Tg-rtTA/TRE-EIF1AX-c'spl* mice fed with regular diet or dox for 4 weeks. Membranes were probed with antibodies to the indicated proteins. Each lane contains a thyroid lobe lysate from a separate mouse.

(D) Western blot showing effect of Si-RNA silencing of ATF4, c-MYC, or both on abundance of AA transporters and on p4EBP1 in C643 vs C643-spl-rev cells.

(E) Co-silencing of ATF4 and c-MYC in dox inducible NthyOri-splice cells disrupted the EIF1AX-splice induction of AA transporters and 4EBP1 phosphorylation.

(F) C643 and C643-spl-rev cells were serum starved overnight, incubated with AA free media for 3h followed by stimulation with glutamine (6mM) and Leucine (2mM). QL stimulated cells lysed at indicated time points were immunoblotted for p4EBP1. Data in B, C, D, E, and F are representative of two independent experiments.

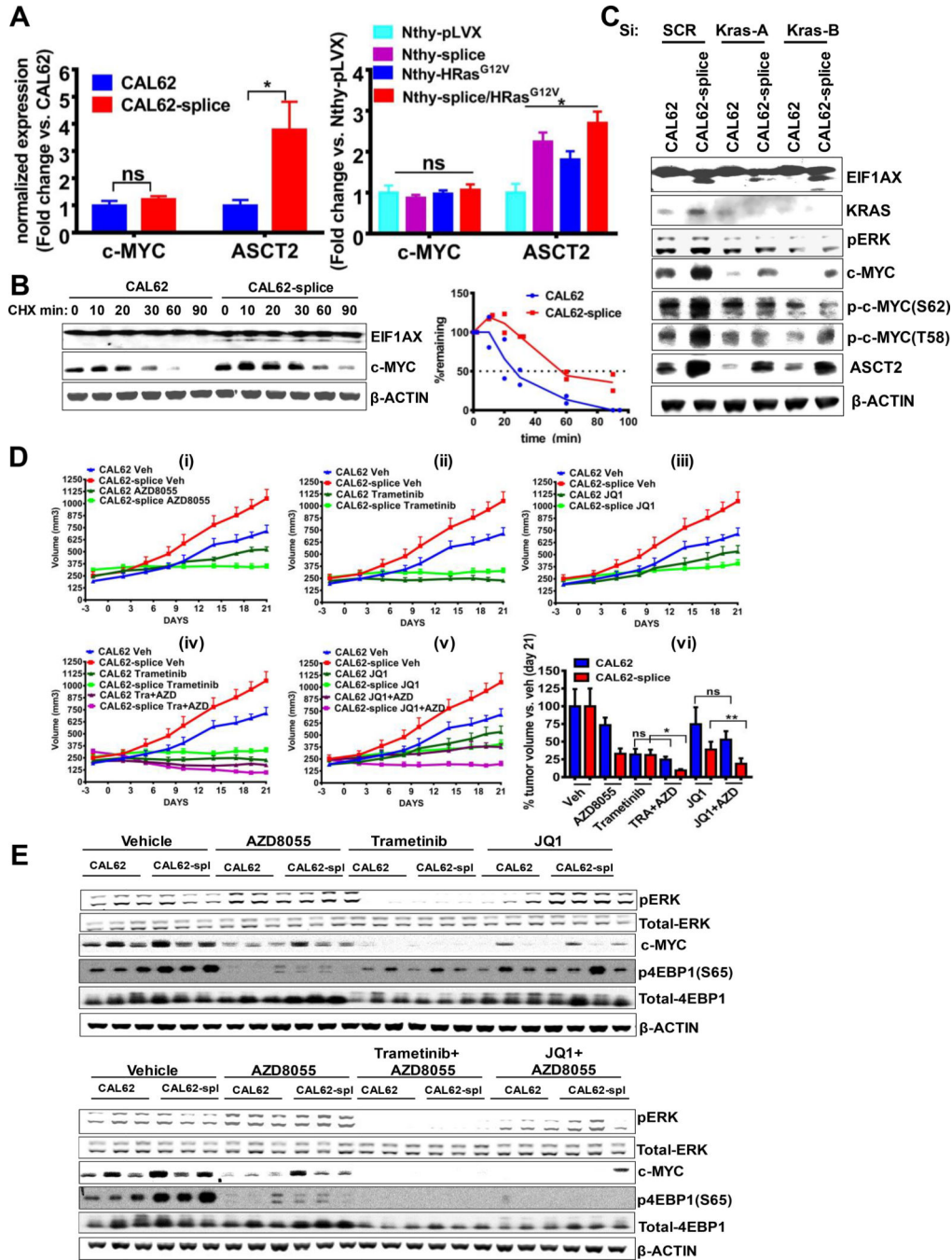


**Figure 6: EIF1AX and RAS mutants converge to stabilize c-MYC, promote mTOR activation and sensitize cells to mTOR, BRD4 and MEK inhibitors.**

(A) RT-PCR of c-MYC and ASCT2 mRNA levels in CAL62 and CAL62-splice cells (*left*) and in dox-inducible NthyOri-splice cells transfected with Hras<sup>G12V</sup> or empty vector (*right*). (B) c-MYC protein half-life determined by cycloheximide (CHX: 100µg/ml) chase in CAL62 and CAL62-splice cells. *Left*: Lysates from cells harvested at the indicated time points after addition of CHX were immunoblotted for c-MYC and actin. *Right*: Half-life of c-MYC was determined by plotting for its degradation over time after normalizing for actin;

c-MYC and  $\beta$ -actin band intensity was quantified using ImageJ software; data points are from two independent experiments.

(C) *Left:* Western blot of CAL62 and CAL62-splice cells transfected with two independent SiRNAs to Kras or a scrambled control (Scr). Knockdown of oncogenic Kras decreased c-MYC abundance and expression of ASCT2.

(D) Effects of the mTOR kinase inhibitor AZD8055, trametinib, or the BRD4 inhibitor JQ1 on CAL62 or CAL62–113splice xenografts in SCID mice. Mice were orally gavaged once a day with vehicle or the indicated drugs at the following concentrations: vehicle: 4% DMSO + 30% PEG300, 10 mg/kg AZD8055, 0.75 mg/kg trametinib or 40 mg/kg JQ1 alone (i,ii,iii) or in combinations (iv,v) for 21 days. Data represent mean with SD of 5 mice/group. vi) Average tumor volume on day 21 with respect to vehicle-treated mice (\*  $p < 0.0009$ , unpaired t test with Welch's correction; \*\* $p < 0.003$ , unpaired t test)

(E) Western blots of the indicated xenograft lysates for pERK, c-MYC, and p4EBP1. Each replicate lysate came from a separate tumor sample.

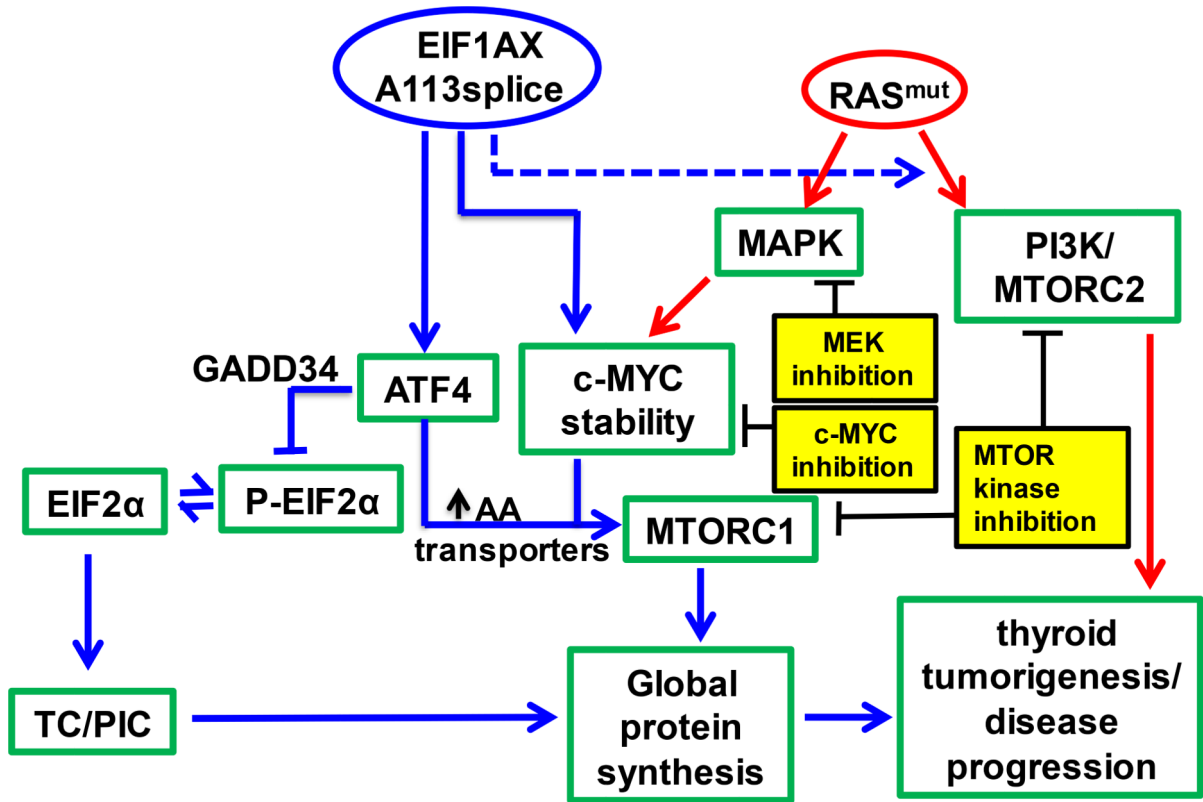


**Figure 7: Mechanism of EIF1AX/RAS co-operation and nodes for targeting**

Mechanisms of mutant *EIF1AX* co-operation with *RAS* in thyroid tumorigenesis. *EIF1AX*-splice activates ATF4 expression, inducing a GADD34/PP1-mediated negative feedback dephosphorylation of EIF2 $\alpha$ , leading to enhanced TC/PIC loading and an increase in global protein synthesis. *RAS* in turn stabilizes c-MYC, an effect augmented by *EIF1AX*-splice. ATF4 and c-MYC induce expression of AA transporters, and cooperate to activate mTORC1. The potential targetable nodes that disrupt the oncogenic drive of *EIF1AX*+ *RAS* are indicated.